Institute of Physical Chemistry
Polish Academy of Sciences
Kasprzaka 44/52
01-224 Warsaw, Poland

PhD Thesis

Shape Transformations of Multicomponent Biological Membranes

Nataliya Bobrovska

Supervisors:

Wojciech Góźdź, D. Sc.
Institute of Physical Chemistry
Polish Academy of Sciences, Poland

Prof. Dr. Aleš Iglič
Faculty of Electrical Engineering
University of Ljubljana, Slovenia

This dissertation was prepared within the International PhD in Chemistry Studies at the Institute of Physical Chemistry of the Polish Academy of Sciences in Warsaw

Project operated within the Foundation for Polish Science International PhD Projects Programme co-financed by the European Regional Development Fund, Operational Program Innovative Economy 2007-2013.

INNOVATIVE ECONOMY
NATIONAL COHESION STRATEGY

FNP
Foundation for Polish Science

EUROPEAN UNION
EUROPEAN REGIONAL
DEVELOPMENT FUND

Warsaw, September 2013

To my beloved parents
and dear friends

Thesis

Segregation of membrane components plays an important role in cellular life and functioning. The primary aim of this thesis is to provide a deeper understanding of the physical mechanisms responsible for the segregation of membranes components in multicomponent biological membranes coupled with the membrane shape transformations.

Diverse functions of cells strongly depend on the shape of the membrane surface and its composition. The lateral distribution of the membrane components on fluid lipid membrane may have a direct influence on cell shape transformations. One of the possible explanations of this phenomenon is based on the hypothesis that the non-homogeneous lateral distribution and segregation of membrane constituents depends on the coupling between the geometry of membrane surface and the non-homogeneous lateral distribution of membrane components. It is assumed that each of the membrane constituents prefers to occupy a membrane region with a membrane curvature comparable to its intrinsic curvature .

The suggested mechanism of non-homogeneous lateral distribution of membrane components may be especially important in the process of formation and stabilization of membrane tubular structures without application of an external pulling/pushing force.

The main goals of this thesis were to check the following hypotheses:

1. ***the change of the membrane shape may cause the lateral redistribution and segregation of membrane components***,
2. ***the formation of membrane tubular structures might be strongly influenced by intrinsic geometry of membrane constituents and their accumulation in a membrane regions with favorable membrane curvature***.

We developed a set of computer programs, which were used to minimize directly the membrane free energy functional within the framework of two theoretical descriptions of membrane elasticity: *the spontaneous-curvature* (SC) model and *the deviatoric elasticity* (DE) model.

The results presented in this thesis show that the lateral redistribution of membrane components may occur only for a certain range of the values of the model parameters such as the vesicle size, vesicle relative volume, area of constituents and their intrinsic

geometry, and elastic moduli of components. The change of vesicle shape may induce the migration of membrane components to the regions with the favorable local curvature that matches better the intrinsic curvatures of membrane components. The lateral distribution of membrane components and the membrane curvature are strongly coupled.

Another an important result of our work is the observation that elongation of the vesicle, following the application of an external force, may lead to the formation of the membrane tubular protrusions, occupied mainly by the component with large spontaneous curvature. Thus, stretching the vesicle can be an effective mechanism of segregation of the membrane components with different intrinsic curvatures.

We have shown that the lateral redistribution and accumulation of anisotropic membrane components may lead to the formation of thin tubular protrusions without the application of active (external) pulling force. It is important to note that, when the membrane components are isotropic, the membrane cylindrical protrusions may be created only due to application of active (external) force.

Acknowledgments

I would like to thank to my mentors Prof. Wojciech Góźdź and Prof. Aleš Iglič for encouraging and motivating me in my scientific journey. I am honored I was given an opportunity to work with them.

I wish to express my gratitude to all my wonderful colleagues and dear friends.

I am deeply grateful to my beloved mother for her endless support, encouragement and patience.

Contents

List of Figures

Introduction

CHAPTER 1

Membranes and their conformations

1.1 Biological membranes - brief introduction

Biological membranes play an essential role in cellular life and functioning. Membrane encloses cell and intercellular organelles (*e.g.* mitochondrion, vesicles, Golgi apparatus) [1]. The compositional *heterogeneity* of biological membranes makes them act as a specialized selective barrier, which separates the interior of the cell/organelle from its exterior, and is responsible for membrane functionality. Membrane functions are as diverse as transporting of nutrient, waste control, encapsulation of larger particles or viruses (phagocitosis, endocitosis, budding) [2, 3], cell locomotion, adhesion to other cells or surfaces (*e.g* adhesion of osteoblasts to titanium implant surface [4]), connections with other cells [5], transmission of information, cell-to-cell communication (*e.g. myelin* is a specialized biological membrane that wraps axon and performs insulating functions [6]). Some basic characteristics of biological membranes are described below.

From the ***structural*** point of view, biological membranes represent a class of *soft (structured) materials* [7]. Biological membrane is a chemically complex self-assembled aggregate, *bilayer*, built of two molecular *monolayers* or *leaflets* [8], in which *lipids*[1], the main building units of biological membrane, are oriented in such a way, that

[1]Lipids belong to the class of molecules called *amphiphiles* (from the Greek: $\alpha\mu\varphi\iota\zeta$ [amphis] – both, $\varphi\iota\lambda\iota\alpha$ [philia] - love) which are composed of two parts: hydrophilic polar head and one (*e. g.* lysophosphatidylcholine) or more (phosphatidylethanolamine (2 tails), monolysocardiolipin (3 tails), cardiolipin (4 tails) or Di[3-deoxy-D-manno-octulosonyl]-lipid A (6 tails), which represents the class TLR-4 Agonist, was recently found in bacteria and macrophage membranes [9–11]) hydrophobic carbon chains (tails), see left-hand side of Fig. 1.2. However, the majority of lipids found in cellular membrane have double chains.

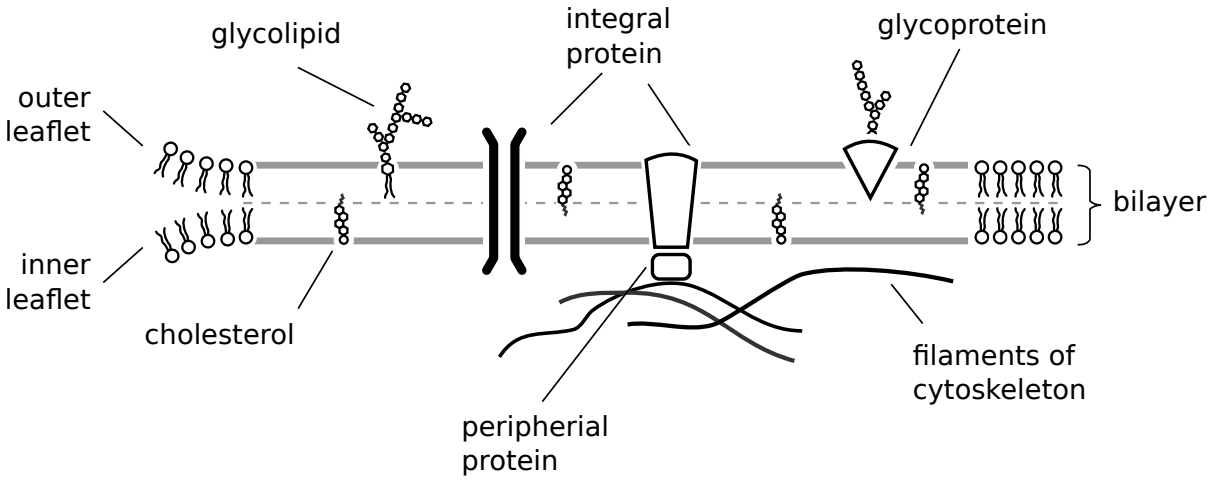

Figure 1.1: A schematic view of the cell membrane with main membrane components: proteins, lipids, cholesterol and attached cytoskeleton.

their hydrophobic chains are situated inside the bilayer, *tail-to-tail* packing (lipid chains create a *hydrophobic core* of the bilayer), when the hydrophilic polar heads are oriented to the outside of bilayer and are in contact with the aqueous environment. Biological membranes are asymmetric [12]. Each cellular monolayer is composed of a heterogeneous collection of lipid and *non-lipid* molecular species, such as proteins, cholesterol etc.[2] (see Fig.1.1), which can freely move (*e.g.* "flip-flop" (lipid exchange between monolayers), rotating, diffusing) in the plane of bilayer due to the thermal motion. The constant thermal motion of molecules within bilayer causes the fluctuation of its shape around some mean value (see Ref. [14] and references within).

From the ***thermodynamical*** point of view, biological membranes may exist in different phases and exhibit different phase transitions. Most of biological membranes

The unique feature - a combination of molecule parts with two opposite characteristics: *hydrophobicity* and *hydrophilicity* was discovered by I. Langmuir (1905) during his studies of the phospholipid monolayer on a water/air interface.). Those properties allows amphiphiles to spontaneous self-assembly into different structures in aqueous solution. Such behavior is induced by a strong water-mediated attraction between hydrophobic tails (the hydrophobic effect is responsible for the aggregation of amphiphilic molecules in water).

Lipids are polymorphic *i.e.* they can create a variety of different kinds of self-assembled structures. In aqueous environment amphiphilic molecules can aggregate into two basic architectures: micelles (spherical and worm-like), Fig. 1.2 (2) and lamellar structures Fig. 1.2 (4) (the preferable structural configuration depends on the concentration of lipids in solution), from which larger and more geometrically complicated structures can be built (uni- or multi-lamellar vesicles, hexagonal and cubic structures etc.). Some of the amphiphilic aggregates are shown in Fig. 1.3

[2]This representation is based on the *fluid mosaic model* for the cell membranes, introduced by S. J. Singer and G. L. Nicolson in 1972 [13].

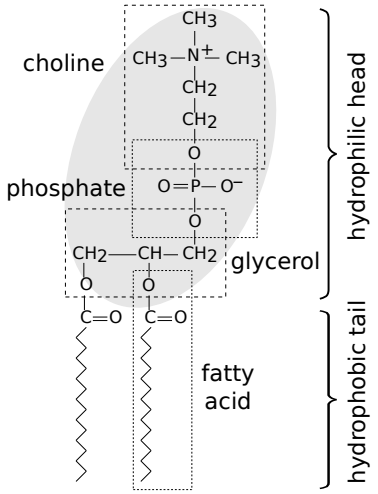

Figure 1.2: Structure of a phospholipid (phosphatidylcholine).

are considered to be in the *fluid* phase[3]. The phase of membrane lipid bilayer depends on the temperature. The main *transition temperature* T_m, depends on the length of the hydrocarbon chains, the degree of saturation of lipid chains and composition of particular membrane (*e.g.* the presence of sterol molecules in one- and multi-component lipid bilayers influences its phase behavior [15, 16]). In biological membranes also different kinds of proteins are embedded in the membrane. Fluid (*liquid crystalline*) phase, L_d or L_α, is characterized by disorder of lipid chains, while in *gel* phase, L_o or L_β, the lipids chains become more ordered. For example, according to the *raft hypothesis* [17], lipid rafts (an organized membrane domains) represent the liquid-ordered phase.

From the ***scale*** point of view, the characteristic feature of biological membranes is the difference between its thickness and size. The thickness of biological membranes, determined by the length of the lipid chains, is thought to be crucial for lateral segregation, concentration and conformation of membrane proteins (see Refs. [18–21] and references within), which, in turn influence protein activation and functionality. Again, lipid rafts (the diameter of raft domain is assumed to be around 50 nm [22]) may serve as an example of local change in membrane organization (thickness) and phase behavior. Membrane thickness may vary from 3 to 5 nm. However,

[3]It is assumed that, in the fluid phase membrane lipid bilayer behaves as an incomprehensible isotropic fluid. The filaments of cytoskeleton attached to the inner surface of lipid bilayer exhibit shear elasticity and cannot be considered as fluid.

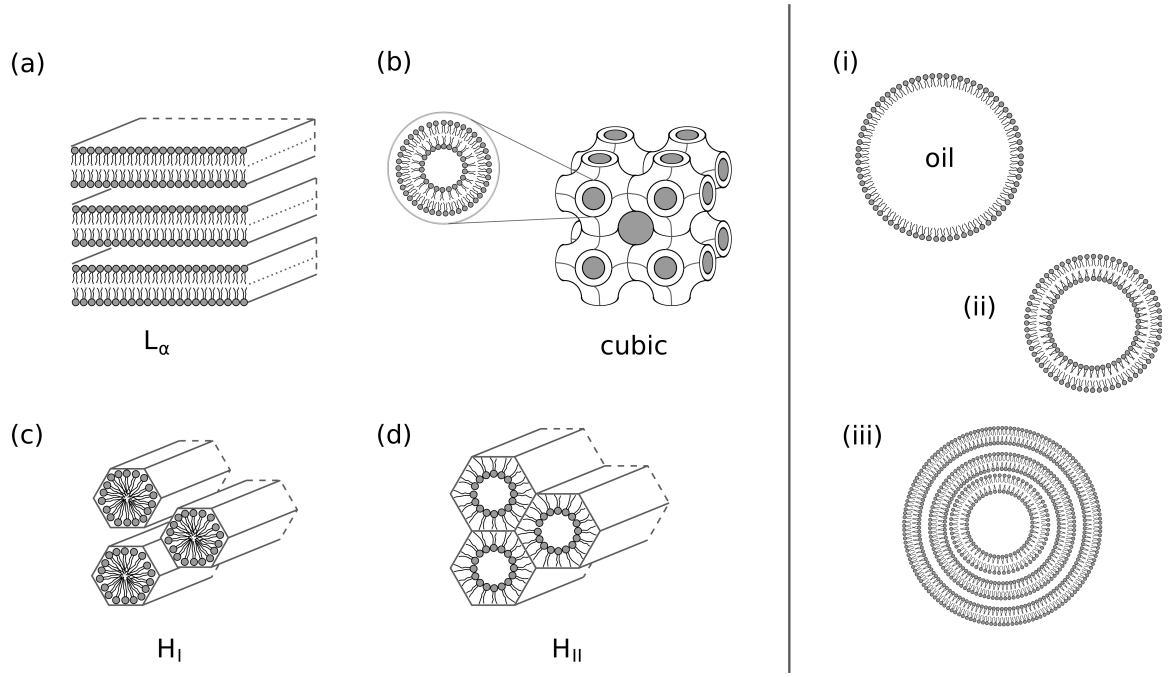

Figure 1.3: Schematic representation of aggregates made by amplilpilic molecules: (a) multilamellar, (b) cubic, (c) hexagonal and (d) inverted hexagonal phases. On scheme (ii) and (iii) the uni- and multi-lamellar vesicles are presented, (i) shows the monolayer vesicle, which is formed on the surface between water and oil.

for closed membrane objects, such as *e.g.* vesicles[4], whose dimensions are several orders of magnitude larger than the membrane thickness, the latter is treated as constant. Moreover, as we shall see in details in Chapter 2, such difference in orders of magnitude allows to apply certain assumptions in the theoretical description of membrane surfaces, which make the elastic continuum approach applicable.

.

1.2 Membrane morphology and component segregation

Membrane heterogeneity is believed to play a crucial role in a number of biological processes such as membrane budding (exocitosis and endocitosis), adhesion, fusion and fission, protein targeting, pore formation, signaling, surface pattering etc. These processes are mostly accompanied by change of the membrane morphology, *which might be partially induced by migration and accumulation of membrane components and their phase separation.*

[4]The diameter of biological membrane vesicles *in vivo* [23] slightly vary in the range of 60 nm. In contrast, the giant unilamellar vesicles (GUVs) may vary from tens nm to tens μm (*e.g.* see Ref. [24]).

Both the composition and the functionality of particular membranes dictate their morphology, thus spherical, ellipsoidal, tubular, toroidal, plane or more geometrically complicated closed membrane structures such as, for example, the myelin-like structures called "Myelin figures"[5] (see Refs. [25, 26] and references within) or helical ribbons can be preset in the cell.

The local composition of biological membranes might be changed during the process of the phase separation or due to the (local) segregation of membrane components induced by the change of the membrane curvature.

The curvature-induced phase segregation of two-component vesicles was theoretically investigated by number of scientists. Lipowsky studied the domain-induced budding of flat membranes and suggested possible influence of coating proteins on the budding mechanism in the natural systems [27]. Later Seifert, by applying the area-difference-elasticity model (ADE), has shown that initially mixed components (one-phase regions) with different geometry can phase segregate due to the transformation of vesicle shape induced by the temperature change [28]. The analysis of the shape deformation of the open-shaped unilamellar planar membranes, close-shaped cylindrical and spherical vesicles with two-phase region is given in Ref. [29, 30]. Julicher and Lipowsky investigated the continuous and discontinuous shape transformations (budding) of vesicles that consist of two fluid domains that are separated by a domain boundary in the framework of spontaneous curvature model (SC) [31]. The importance of an orientation of anisotropic membrane inclusions which induce spontaneous deviatoric bendings in lipid bilayer was shown by M. Fischer [32], J. B. Fournier [33] and V. Kralj-Iglič [34].

1.3 Concept of nanodomains in lipid membranes

As was mentioned above, different functions of biological membranes may be activated by the mechanisms responsible for the segregation of membrane components induced by the change of the membrane curvature [35, 36]. The change of the membrane curvature might be also induced by the geometry of the membrane constituents.

The intrinsic architecture of a lipid bilayer is governed by its composition, where

[5]The "Myelin figures" are an infinite planar bilayr structures with a concentric or a whorl-like shapes, which remind the myelin coating (Schwan cell) of nerve axon.

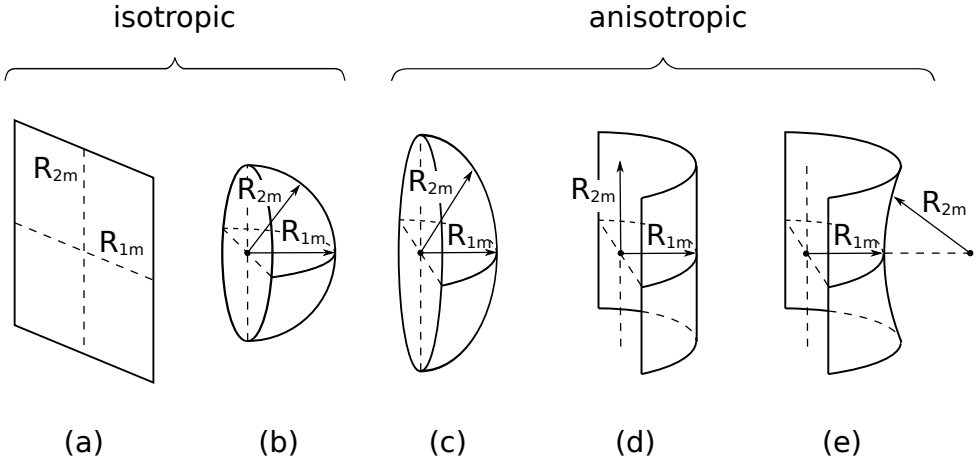

Figure 1.4: Possible geometries of membrane nanodomain characterized by its intrinsic principal radii R_{1m} and R_{2m}, which are linked with the intrinsic spontaneous curvatures by $C_{im} = 1/R_{im}$, $(i = 1, 2)$. (a) Flat ($C_{1m} = C_{2m} = 0$), and (b) spherical($C_{1m} = C_{2m} \neq 0$), nanodomains correspond to the rotationally symmetric membrane components (*isotropic*), and set of (c) ellipsoidal ($C_{1m} \neq C_{2m} > 0$) and ($C_{1m} \neq C_{2m} < 0$), (d) cylindrical ($C_{1m} \neq 0$, $C_{2m} = 0$), and (e) saddle-like ($C_{1m} > 0$, $C_{2m} < 0$) or ($C_{1m} > 0$, $C_{2m} < 0$) nanodomains corresponds to the non-rotationally symmetric membrane components (*anisotropic*).

the key role plays the intrinsic shape of it's basic building blocks, membrane constituents, and the interactions between them. In multicomponent membranes some molecules can form *nanodomains*.

Nanodomain can be understood as a large macromolecule, which is (laterally) placed in the bilayer, or a bilayer small stable aggregations of cluster of molecules, which are composed of: lipids of one kind; other non-lipid molecules of one kind; mixture of different kinds of lipids; mixture of lipids and other molecules; or mixture of different molecules.

Macromolecules, like proteins, are much larger than lipid molecules, and may form complexes with a large number of lipids. Such a complex can be considered as a membrane component with much larger size then the area of single lipid molecule. Some macromolecules, bound to the membrane surface, may induce the change of bilayer curvature. Such process shows the coupling between local curvature of the bilayer and the local concentration of the mecromolecules [37].

Nanodomains can be characterized by different shape geometry with rotational (*isotropic* nanodomains ($C_{1m} = C_{2m}$)), and non-rotational symmetry (*anisotropic* nanodomains ($C_{1m} \neq C_{2m}$)), (Fig. 1.4) [38].

1.4 Possible mechanisms of segregation of membrane components

The heterogeneous biological membranes may be in the first approximation considered as two dimensional (2D) liquids [39]. The membrane components can be mixed or phase separated [40, 41]. When attraction between components of the same kind is significantly stronger than the interaction between components of different kind, then the energy gain associated with separation of the components competes with the entropy loss. At low enough temperature and low mobility of membrane components the entropy plays a less important role and phase separation takes place. In the case of comparable intermolecular interactions between the components of different kinds or high temperature no thermodynamic phase separation occurs. Still, segregation of the components of the membrane forming a closed vesicle might occur if one component is characterized by large and the other one by small spontaneous curvature. The energy cost due to the difference between local and spontaneous membrane curvature contributes to the bending energy of the membrane described within Helfrich theory [42]. When the component with large intrinsic curvature occupies regions characterized by relative large local curvature and the other component with the small intrinsic curvature occupies regions characterized by relative small local curvature, the elastic energy decreases compared to the case of homogeneously mixed components.

Segregation of the membrane components induced by coupling between the shape of the vesicle and the lateral concentration was predicted based on the above considerations in several works [35, 40, 43–49]. On theoretical grounds the question of shape-induced segregation of the components on the vesicle membrane was investigated in Refs. [28,50]. An axisymmetric vesicle composed of two types of lipids, with different local concentration in outer and inner monolayer was studied in Ref. [28] in the modified area-difference-elasticity model. In the model it was assumed that the local concentration difference between outer and inner monolayer, $\phi(s)$, induces local spontaneous curvature of the bilayer at the position parmeterized by s (where s is an arclength) due to different molecular architectures of the two components. In addition, the combined effect of intermolecular interactions and entropy of mixing was included according to the Landau theory of the demixing transition. Namely,

the term proportional to $\phi^2(s)$ integrated over the surface of the vesicle, with positive proportionality constant in the one-phase region, was added to the elastic energy. The Landau theory is valid close to the critical point, where the order parameter ϕ is small, therefore the model studied in Ref. [28] is valid only in the weak segregation limit. Indeed, for reasonable model parameters the variation in composition associated with budding (dividing the vesicle into low- and high-curvature parts) was found to be 1% and 10% for the vesicles with radius $R = 1\mu m$ and $100nm$ respectively. The above results indicate that in the case of two types of lipids the curvature-composition coupling is not an effective mechanism of segregation of the components.

1.5 The goals of the thesis

This work is devoted to understanding the mechanisms responsible for segregation of membrane components, which in turn, influences the shape transformations and functionality of biological membrane systems.

The *segregation* of components and nanodoamins in multicomponent membranes can arise under certain conditions. One possibility is that membrane components, which are characterized by different spontaneous (intrinsic) curvatures and neutral intermolecular interactions, might affect the membrane curvature, trying to fit it to their own curvature by the partial or full accumulation in the favorable membrane region(s) , as a consequence the membrane changes its shape [35]. The other possibility is that the membrane components accumulate in the membrane regions with the curvature comparable to their own intrinsic curvature but do not significantly change the membrane shape, i.e. the membrane geometry remains more or less fixed [43].

The structural complexity of biological membranes makes their investigation highly difficult, therefore it is convenient to use the simplified *model membrane system*, which might be described theoretically.

In this thesis, two different theoretical descriptions (*spontaneous-curvature model* and *deviatoric-elasticity model*) of the biological membranes are used for the *numerical* investigation of processes governing the shape transformations of membranes surface coupled to membrane component lateral redistribution and segregation. *Two-component* model membrane system, which forms closed hollow *vesicles* with spherical topology, is considered for the sake of simplicity.

The main goals of the thesis are:

- Further verification of the hypothesis, that the change of the membrane shape may cause segregation of membrane components.
- Further verification of the hypothesis, that the formation of membrane tubular structures might be driven by the intrinsic geometry of membrane constituents and the application of external force is not necessary.

We hope that the results of the proposed thesis will be helpful in better understanding the mechanisms of lateral redistribution and segregation of membrane components in biological membranes.

1.6 Organization of the thesis

Chapter 2 is devoted to a theoretical description of the spontaneous curvature model and the deviatoric elasticity model of biological and model lipid bilayer membranes.

In Chapter 3 the mathematical representation of axially symmetric vesicle surface and the corresponding expression for the membrane free energy for two-component membrane vesicles are introduced. The approximate functions for the local concentration of the membrane components are presented.

In Chapter 4 the numerical investigations of lateral redistribution and segregation of membrane components in two-component vesicle membrane using the spontaneous curvature model is given. It is assumed that membrane components are isotropic and characterized by different spontaneous curvatures.

In Chapter 5 the studies concerning the formation of tubular membrane structures induced by the accumulation of the anisotropic membrane component in the membrane region with large curvature (vesicle neck or protrusion) are presented. It is assumed that membrane is composed of the mixture of isotropic and anisotropic components or only anisotropic components, which are characterized by different intrinsic deviatoric curvatures. The calculations were performed using the deviatoric elasticity model.

In Chapter 6 the obtained results of the thesis are summarized and the main conclusions are presented.

CHAPTER 2

Theoretical models of biological membranes

The difficulty in explanation of the variety of shapes observed in the red blood cells (RBCs), such as discocyte (biconcave structure), stomatocyte or ehinocyte, and the unusual behavior of RBC's membrane have attracted great scientific interest since the end of XIX century, when Hamburger (1895) described the reversible shape change of RBC from a biconcave disc into a crenated sphere.

Since that time thousands of papers dedicated to the experimental, theoretical and numerical investigations of mechanisms governing the morphological changes of RBC membrane and other bilayer membrane systems have been published. Nevertheless, the biological membranes still remain one of the most intriguing systems created by nature and the phenomena and mechanisms, which are observed in such systems, are still puzzling the scientists involved in these investigations.

This Chapter presents two theoretical models describing the mechanics of fluid-like lipid membranes considering the intrinsic geometry of membrane constituents, which might be characterized by rotational (isotropic) and non-rotational (anisotropic) symmetry. In Secs. 2.1 and 2.2, the *spontaneous curvature* (SC) and the more general *deviatoric elasticity* (DE) models are described.

2.1 Spontaneous-curvature model

The shape transformations of biological membranes (mechanics) has been intensively studied for more than four decades. Nevertheless, due to high complexity in the

composition of biological membranes, the most studies in this field are restricted to simplified, so-called, *model membrane systems*, which represent lipid bilayer, consisting of one or more components and tend to mimic real biological membrane systems. Such simple systems allow to focus on basic physical aspects concerning biological membranes [51], and may serve as the material for artificial cells [52]. However, one should understand how big the difference between biological membranes and model membrane systems is.

One of the important roles in mechanics of membrane shape transformation plays *membrane curvature* (for brief review see [53] and references within).

The connection between membrane curvature and its "bending resistance" in RBCs was first emphasized by Rand and Burton (1964), who examined experimentally the unusual behavior of RBCs and determined the resistance to deformation of the red cell membrane [54]. In 1966 Fung discussed the general relation between bending resistance and membrane tensions and pointed out the importance of bending in stability of the biconcave shape of red cells when they are stressed [55].

One of the successful attempts of theoretical explanation of membrane shapes observed in RBCs was made by Canham in 1970 [56], who proposed the theory of the stable RBC shapes based on minimization of membrane bending energy. He has shown that the biconcave shape of the red blood cell (RBC) can be described by the bending energy

$$U = \frac{D}{2} \int \left(\frac{1}{R_1^2} + \frac{1}{R_2^2} \right) dS, \tag{2.1}$$

where R_1 and R_2 are the principal curvatures of the membrane mid surface at a given point, D is the bending rigidity, E it the Young's modulus, h is the membrane thickness, ν is the Poisson's ratio, and dS is an infinitesimal surface area element. However, this theory gives only an approximate solution.

In 1973 W. Helfrich [42] formulated a theory of the elasticity of lipid bilayer, based on the assumption of unrestricted internal fluidity of membrane, which implies vanishing shear modulus. Thus, the membrane is treated as a two-dimensional fluid. Such consideration of the lipid bilayer requires the examination of stretching, tilt, and curvature, the three kinds of strains affecting the membrane elasticity. The change of the membrane thickness, h, is not taken into consideration. It is assumed that the membrane is homogeneous over the entire surface. Such assumption allows to consider the membrane as a two-dimensional surface embedded into 3D Euclidean

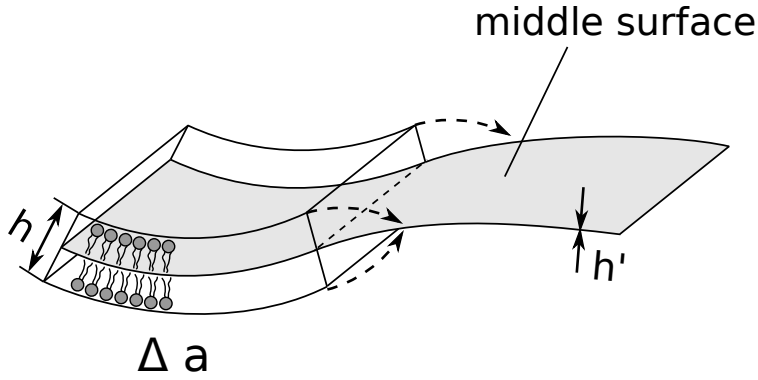

Figure 2.1: Simplified schematic sketch of an element of membrane with a surface area Δa, membrane thickness h, which tends to be infinitesimally thin, $h \longrightarrow h'$, and the principal radii of curvature, R_1 and R_2.

space and to describe it within a continuous-mechanical approach (Fig. 2.1).

The membrane local bending energy was written as [42]

$$F_b^{\mathrm{SC}} = \frac{\kappa}{2} \int (C_1 + C_2 - C_0)^2 \, dS + \bar{\kappa} \int C_1 C_2 dS, \tag{2.2}$$

where κ and $\bar{\kappa}$ are the bending moduli, C_1 and C_2 are the membrane principal curvatures, which characterized geometrical surface (vesicle surface, S) at each point, C_0 is the *spontaneous curvature* of membrane (with dimensionality of the principle curvature), dS is the infinitesimal membrane area element. For closed surfaces with fixed topology last term on the right-hand side of Eq. (2.2) is constant according to the Gauss-Bonnet theorem, see App. A.2). The spontaneous curvature C_0 denotes an intrinsic asymmetry[1] of membrane bilayer showing that in relaxed state membrane is curved (not flat).

In 1974 E. A. Evans [57] studied a possible mechanism for crenation of red blood cells for connected and unconnected bilayers. He came to the conclusion that for connected bilayer the bending resistance is a function of a local curvature of the bilayer and its free energy is a sum of the chemically induced moment free energy and the bending resistance. The last term, $D/2(1/R_1 + 1/R_2)^2$, takes similar form of one proposed by Canham and Helfrich (D is the bending rigidity constant).

The theoretical description of biological membrane proposed by Canham, Helfrich and Evans is called the *spontaneous curvature model* (SC). The SC model was successful

[1]For example, the membrane asymmetry might be induced by the difference in composition of inner and outer monolayers or by attaching the macromolecule to the bilayer.

in explaining shapes of RBCs[2].

2.2 Deviatoric Elasticity model

The problem of tubular structures in the biological membranes has attracted a great interest since the end (late 70's) of the XXth century, since they play an important role in intracellular [1,59] and "outer-cellular" processes, such as intercellular communication [60–62] or material transportation. It seems to be closely connected with the studies of multicomponent biomembrane systems.

The first theoretical attempts to explain the formation of tubular structures that have been found in the membrane solid state (tubes and helical ribbons) were made independently by Helfrich and de Genes (1987). In 1988, Helfrich inspired by experimental data, put forward the suggestion that the solid bilayers have to be anisotropic to be able to form tubular and ribbon-ike structures [63]. Further theoretical investigations were made by Fisher (1992) [64]. In his work the author, following Evans and Skalak [65], considered the spontaneous curvature as the superposition of the isotropic and deviatoric contributions. The deviatoric contribution or *deviator of the local curvature*, was denoted as antisymmetric part of expression for Gaussian curvature, $((C_1 - C_2)/2)^2$.

$$\bar{k}_c C_1 C_2 = \bar{k}_c \left\{ \left(\frac{C_1 + C_2}{2} \right)^2 - \left(\frac{C_1 - C_2}{2} \right)^2 \right\}. \tag{2.3}$$

Fisher also pointed that for a non zero deviatoric contribution the total spontaneous curvature of the molecules (intrinsic spontaneous curvature) must be anisotropic, i.e. the molecules must not have rotational symmetry as it is in the isotropic case, when the deviatoric contribution is equal zero.

In 1996 Kralj-Iglič *et al.* proposed a *deviatoric elasticity model* (DE), where the anisotropic properties of membrane constituents are taken into account [34]. The brief introduction to DE model is given in Section 2.2.1.

[2] In 1976 H.J. Deuling et W. Helfrich obtained a catalogue of large variety of rotationally symmetric shapes of vesicles (made of closed fluid membranes) [58]. This work served as a verification of proposed earlier theoretical model of membrane elasticity, SC model. Shapes (for one-component membrane) were calculated as a function of enclosed volume, membrane area and spontaneous curvature. By taking the area as a constant, $S = const$, the authors emphasized that the only parameter controlling the shapes of the vesicles is the curvature of membrane.

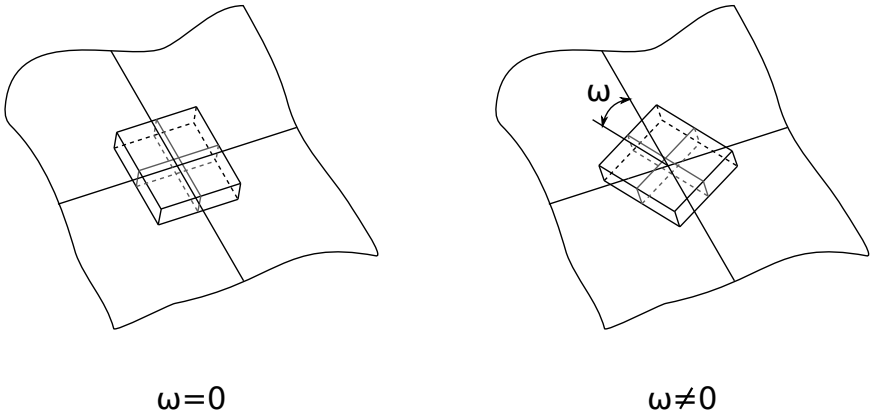

Figure 2.2: Schematic sketch of a rotating membrane element with area a_0. ω is the angle of rotation of membrane element.

2.2.1 Formalism of DE

Consider a small plate-like membrane element (*e.g.* inclusion or nanodomain) with area a_0 (Fig. 2.2). The elastic energy of such element is the energy of the mismatch between the actual local curvature of the membrane and the *intrinsic* (spontaneous) curvature of the nanodomain .

According to [66,67], the *mismatch* tensor is defined as $\underline{M} = \underline{R}\ \underline{C}_{\mathrm{m}}\underline{R}^{-1} - \underline{C}$, where the tensor $\underline{C}$ describes the actual local membrane curvature, tensor $\underline{C}_{\mathrm{m}}$ describes the *intrinsic* curvature of the inclusion, and the rotational matrix takes the form

$$\underline{R} = \begin{bmatrix} \cos\omega & -\sin\omega \\ \sin\omega & \cos\omega \end{bmatrix}, \tag{2.4}$$

where ω is the angle of rotation of the membrane element (please note, that all orientations of a single membrane element do not have the same energy), see Fig. 2.2.

The curvature tensors are defined as

$$\underline{C} = \begin{bmatrix} C_1 & 0 \\ 0 & C_2 \end{bmatrix}, \quad \underline{C}_{\mathrm{m}} = \begin{bmatrix} C_{1\mathrm{m}} & 0 \\ 0 & C_{2\mathrm{m}} \end{bmatrix}. \tag{2.5}$$

The elastic energy of the membrane element per unit area w should be a scalar quantity. Therefore each term in the expression for w must also be a scalar [68], *i.e. invariant* with respect to all transformations of the local coordinate system. The expression for w is approximated by an expansion in powers of all independent

invariants of the mismatch tensor $\underline{M}$ up to the second order in the components of $\underline{M}$.

$$w = \mu_0 + \frac{K_1}{2}(\mathrm{Tr}\underline{M})^2 + K_2\,\mathrm{Det}\underline{M}, \tag{2.6}$$

where μ_0 is the minimal possible value of w, while K_1 and K_2 are constants. For the sake of simplicity we take $\mu_0 = 0$.

Finally, the elastic energy per membrane element is

$$w = (2K_1 + K_2)(H - H_m)^2 - K_2(D^2 - 2DD_m\cos(2\omega) + D_m^2), \tag{2.7}$$

where $H = (C_1 + C_2)/2$ and $H_m = (C_{1m} + C_{2m})/2$ are the *mean* and the *intrinsic mean curvatures*, respectively, whereas $D = |C_1 - C_2|/2$ and $D_m = |C_{1m} - C_{2m}|/2$ are the *curvature deviator* and the *intrinsic curvature deviator*, respectively. Derivations for Eq. (2.7) are given in Appendix B.

2.2.2 Limiting case of deviatoric elasticity model

The Eq. (2.7), considered in Section 2.2.1, represents a *general form* of bending energy for membrane element, which takes into account *anisotropy* of components. For *isotropic* membrane components the intrinsic principal curvatures are equal $C_{1m} = C_{2m} = C_m$, and therefore $D_m = 0$ and $H_m = C_m$ (see Appendix C).

$$w_{lim} = \underbrace{\left\{\left[\frac{K_1}{2}4H^2 - \left(\frac{2K_1 + K_2}{2}\right)4HH_m + \cdots\right] + K_2C_1C_2\right\}}_{Helfrich\ form} + (2K_1 + K_2)H_m^2, \tag{2.8}$$

where $H_m = (K_1C_0)/(2K_1 + K_2)$.

The expression (2.8) can be rewritten in the form of SC model

$$w_{lim} = \left\{\frac{K_1}{2}(H - C_0)^2 + K_2C_1C_2\right\} - \frac{(K_1^2 - K_2)}{2K_1 + K_2}C_0^2, \tag{2.9}$$

where term $[(K_1^2 - K_2)/(2K_1 + K_2)]C_0^2$ does not depend on H (is *constant*) and can be omitted. The spontaneous curvature is $C_0 = H_m(2K_1 + K_2)/K_1$.

CHAPTER 3

Mathematical description of vesicle surface in the case of rotational symmetry

3.1 Parameterization of vesicle shape

In this Thesis we consider only axisymmetric vesicles[1], thus the vesicle surface is a *surface of revolution*, which assumes rotational symmetry about the z-axis (the angle of rotation is in the range $0 \leq \Psi \leq 2\pi$). To describe vesicle surface with rotational symmetry, it is enough to write parameterization only for a plane curve (profile) of the vesicle, which is characterized by an arclength s and an angle of the tangent to the profile with the plane perpendicular to the axis of rotation z, $\theta(s)$, see Fig. 3.1.

The infinitesimal height $dz(s)$ and the elementary radius $dr(s)$ are

$$dz(s) = \sin\theta(s)ds, \qquad dr(s) = \cos\theta(s)ds.$$

and therefore the parametric equations of the vesicle profile are

$$z(s) = \int_0^s \sin\theta(s')ds', \tag{3.1}$$

$$r(s) = \int_0^s \cos\theta(s')ds'. \tag{3.2}$$

[1] for the simplicity of calculations

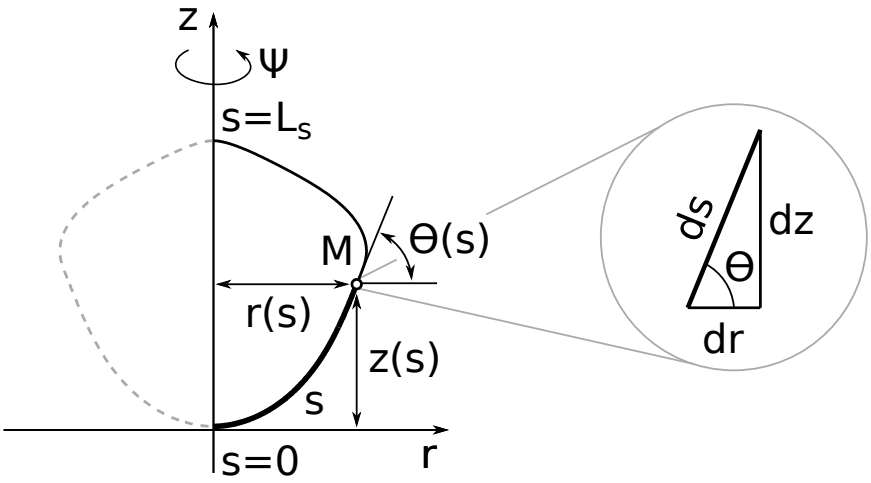

Figure 3.1: Schematic representation of a vesicle profile with a curve element, ds. $r(s)$ and $z(s)$ are the coordinates of point M, Ψ is the angle of rotation, $\theta(s)$ is the angle between the tangent to the profile with the plane perpendicular to the axis of rotation, z, and L_s is the length of the profile.

The boundary conditions necessary for the parameterization of a closed shape [69]

$$\theta(0) = 0, \quad \theta(L_s) = \pi, \quad r(0) = 0, \quad r(L_s) = 0. \tag{3.3}$$

The function $\theta(s)$ is expanded in a Fourier series [69]:

$$\theta(s) = \frac{\theta_0}{L_s} s + \sum_{n=1}^{N} a_n \sin\left(\frac{n\pi}{L_s} s\right), \tag{3.4}$$

where $\theta_0 = \pi$ when the shape of the vesicle without up-down symmetry is parameterized, L_s is the length of the shape profile, N is the number of the Fourier modes and a_n are the Fourier amplitudes.

3.2 The expressions for principal curvatures C_1 and C_2

In the 3D Euclidean space, the vector describing the points on a surface of revolution is written as $\mathbf{R} = \{r\cos\psi, r\sin\psi, z\}$ [2]. In case, when the profile is parameterized by $\theta(s)$, it takes the form

$$\mathbf{R} = \{r(\theta(s))\cos\psi, r(\theta(s))\sin\psi, z(\theta(s))\} \tag{3.5}$$

where the angle of rotation ψ and the arclength s are coordinates on the surface.

The recipe of calculation of the principal curvatures C_1 and C_2 is presented below.

[2]For the simplicity of description from now on in some cases we will write z, r, θ instead of $z(s)$, $r(s)$, $\theta(s)$.

1. The metric tensor g_{ij} is calculated as [70]:

$$g_{ij} = \begin{pmatrix} \frac{\partial \mathbf{R}}{\partial s} \cdot \frac{\partial \mathbf{R}}{\partial s} & \frac{\partial \mathbf{R}}{\partial \psi} \cdot \frac{\partial \mathbf{R}}{\partial s} \\ \frac{\partial \mathbf{R}}{\partial s} \cdot \frac{\partial \mathbf{R}}{\partial \psi} & \frac{\partial \mathbf{R}}{\partial \psi} \cdot \frac{\partial \mathbf{R}}{\partial \psi} \end{pmatrix} = \begin{pmatrix} 1 & 0 \\ 0 & r^2 \end{pmatrix}, \tag{3.6}$$

where

$$\partial \mathbf{R}/\partial s = \{\cos\theta \cos\psi, \cos\theta \sin\psi, \sin\theta\} \tag{3.7}$$

$$\partial \mathbf{R}/\partial \psi = \{-r \sin\psi, r \cos\psi, 0\} \tag{3.8}$$

2. The unit normal $\mathbf{n}$, defined as $\mathbf{n} = (\partial \mathbf{R}/\partial s \times \partial \mathbf{R}/\partial \psi)/\sqrt{\det(g_{ij})}$, is

$$\mathbf{n} = \{-\cos\psi \ \sin\theta, -\sin\psi \ \sin\theta, \cos\theta\} \tag{3.9}$$

3. A supporting matrix $\mathbf{Y}$ takes form

$$\mathbf{Y} = \begin{pmatrix} \frac{\partial^2 \mathbf{R}}{\partial s^2} & \frac{\partial^2 \mathbf{R}}{\partial s \partial \psi} \\ \frac{\partial^2 \mathbf{R}}{\partial \psi \partial s} & \frac{\partial^2 \mathbf{R}}{\partial \psi^2} \end{pmatrix}. \tag{3.10}$$

4. The coefficients of the second fundamental form, L_{ij}, are defined as follows

$$L_{ij} = \mathbf{Y} \cdot \mathbf{n}. \tag{3.11}$$

5. The curvature tensor H_{ij} is then

$$H_{ij} = {g_{ij}}^{-1} L_{ij} = \begin{pmatrix} \frac{d\theta}{ds} & 0 \\ 0 & \frac{\sin\theta}{r} \end{pmatrix}. \tag{3.12}$$

Finally, the principal curvatures for a given parameterization are

$$C_1 = C_1(s) = \frac{d\theta(s)}{ds}, \qquad C_2 = C_2(s) = \frac{\sin(\theta(s))}{r(s)}. \tag{3.13}$$

3.3 Calculation of bending energy

The general expression for bending energy F_b for the profile parameterized with the function $\theta(s)$ is given by the following formula

$$F_b = F_b[\theta(s)] = \int_0^{2\pi} d\psi \int_0^{L_s} \mathcal{H}(s) r(s) ds, \tag{3.14}$$

where ψ is the angle of rotation as shown on Fig.3.1, $\mathcal{H}(s)$ is the Hamiltonian, which corresponds to the appropriate form for each theoretical model.

For instance, for one-component case of SC model it will take the form $\mathcal{H}(s) = (\kappa/2)(C_1(s) + C_2(s) - C_0)^2$.

The *surface area* and the *volume* of the vesicle are calculated as

$$S = 2\pi \int_0^{L_s} r(s)ds, \tag{3.15}$$

$$V = \pi \int_0^{L_s} r^2(s) \sin\theta(s)ds, \tag{3.16}$$

respectively.

Due to the insertion of the Eq. (3.4) into Eqs. (3.1), (3.2) and (3.14), the functional minimization can be replaced by the minimization of the function of many variables. The functional (3.14) becomes the function of the amplitudes a_i and the length of the shape profile L_s. In numerical minimization the shape profile is expanded into an appropriate Fourier series and the resulting functional is minimized with respect to the coefficients in the Fourier expansion, Eq. 3.4.

3.4 Calculation of membrane free energy

To study *multicomponent* membrane systems, we propose a model with the entropy having the form of the *entropy of mixing* that is not limited to a weak segregation limit. The surface area of nanodomains is taken into account as a model parameter, and the elastic energy depends on the spontaneous curvature that is, in turn, related to the *concentration* of the macromolecules.

This work is an attempt to answer the question, if the nanodomains can be segregated by the morphological transformations of the vesicle shape[3].

The mechanisms of the shape transformations for vesicles with fixed membrane area, considered in this work, might be induced

- *by the change of the reduced volume* [4] of the vesicle,
- due to the application of the *external force*,

[3]The axially symmetrical vesicles are studied within the framework of spontaneous-curvature (SC) and deviatoric elasticity (DE) models.

[4]The dimensionless *reduced volume* $v = V/V_0$ is defined as the ratio of the volume inside the investigated vesicle, V, to the volume of the sphere with the same surface area as the surface of the investigated vesicle, $V_0 = (4/3)\pi R_0^3$, where $R_0 = \sqrt{S/4\pi}$ is the radius of the sphere. R_0 is used to set up the length scale, and the values of the curvatures are reported in $1/R$ units. In addition, the dimensionless spontaneous curvature c_0 is defined as $c_0 = C_0 R_0$.

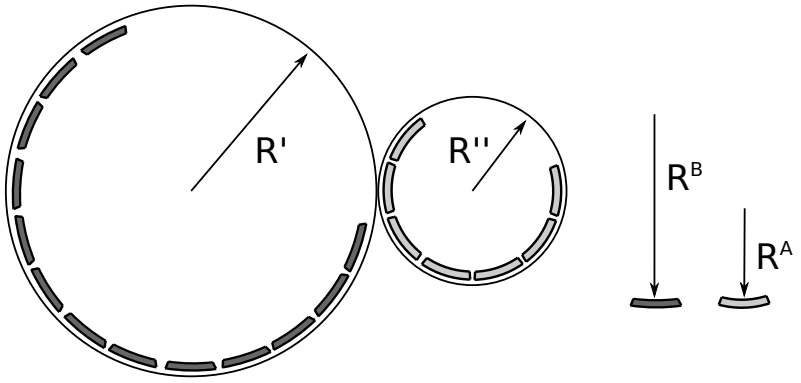

Figure 3.2: Schematic illustration of surface preferable curvatures for components A (light gray) and B (dark gray) ($1/R''$ and $1/R'$) according to their own intrinsic curvatures ($C^A = 1/R^A$ and $C^B = 1/R^B$). R^j ($j = A, B, \prime, \prime\prime$) are the principal radii.

- by the change of membrane component *concentration* (in two-component vesicles),
- by the change of the *intrinsic shape* of components

We find that lateral separation of the membrane components depends strongly on the surface area of nanodomains. The increasing of the area of the complex (nanodomain) induces stronger segregation of components.

We consider the membrane as a surface composed of fixed total number of nanodomains. Single nanodomain surface area is a_0, while nanodomain radii of curvature are R^A and R^B as schematically shown on Fig. 3.2. The molecular packing and the stretching energy of the membrane is not taken into account.

In our studies we investigate two-component axially symmetric closed bilayer vesicles, where the intrinsic shapes of membrane components (nanodomains) A and B are characterized by spontaneous curvatures C_0^A and C_0^B, mean intrinsic curvatures H^A, H^B , intrinsic curvature deviators D^A, D^B and bending rigidities κ^A and κ^B. The total relative concentration is $\phi_A + \phi_B = 1$, where ϕ_A and ϕ_B are concentrations of components A and B, respectively. We denote the concentration of component A as ϕ and the concentration of component B as $(1 - \phi)$.

In all performed calculations, the equilibrium shapes correspond to the minimum of the membrane total energy at constant values of the membrane surface area S and the vesicle volume V, which can be written in the generalized form

$$F_{tot} = F_b + F_{mix}, \tag{3.17}$$

where the expression for the bending energy F_b is given by Eq. 3.14.

The *free energy* associated with the entropy of mixing is given by

$$F_{mix} = \frac{k_B T}{a_0} \int [\phi \ln \phi + (1-\phi) \ln(1-\phi)] dS, \tag{3.18}$$

where T is temperature, k_B is the Boltzmann constant and ϕ is the concentration of the component A. The integral is taken over the whole surface of the vesicle membrane, S.

The relative importance of the two terms in Eq. 3.17 depends crucially on the value of the area of single nanodomain a_0. The role of the entropy of mixing *increases* with the *decreasing* of the nanodomain area, since the number of nanodomains is increased.

The functional for membrane total energy F_{tot} is minimized with the *constraints* on :

- total concentration of components $\phi_{tot} = 1/S \int \phi dS$,
- surface area S and
- volume of the vesicle V.

We do not solve Euler-Lagrange equations but *numerically* minimize the functional as described in Ref. [41,69,71]. As a result of the minimization, we obtain the function $\theta(s)$ which determines the shape of the vesicle (see Fig. 3.1), and the function $\phi(s)$ which determines the concentration profile.

3.5 The function describing the local concentration of components.

The *local (relative) concentration* of membrane components is described by two different functions, $\phi'(s)$ and $\phi''(s)$, which schematically are shown in Fig.3.3,

$$\phi'(s) = \frac{1}{2}\Delta\phi \left[1 - \tanh\left(\xi\left(s - s_0\right)\right)\right] + \phi_1^A, \tag{3.19}$$

$$\phi''(s) = \frac{1}{2}\Delta\phi \left[\tanh\left(\xi\left(s - s_0\right)\right) - \tanh\left(\xi\left(s - s_0 - \Delta s_0\right)\right)\right] + \phi_1^A, \tag{3.20}$$

where s is the profile arclength, s_0 is the position of the boundary between the region rich in component A and the region rich in component B, ξ is the slope of the concentration profile at s_0, Δs_0 is a distance between inflection points of two hyperbolic tangents.

The functions are constructed in such a way that allows the formation of one or two regions on the membrane surface with the different local concentrations of component A, ϕ_1^A and ϕ_2^A. The *concentration difference* is denoted as $\Delta\phi = \phi_2^A - \phi_1^A$.

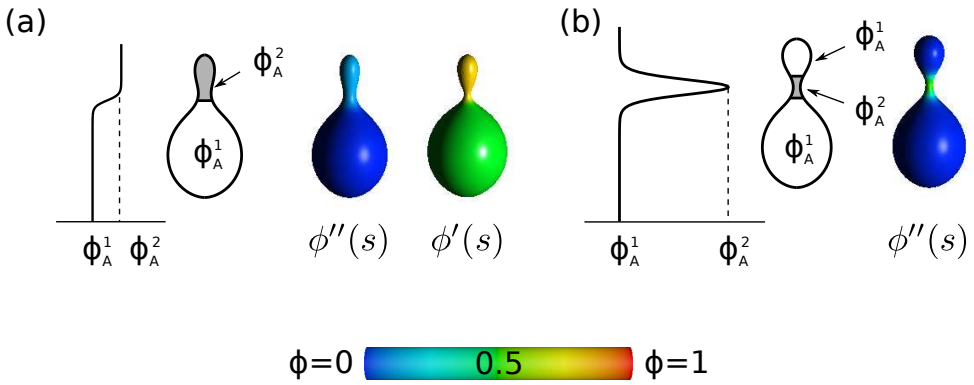

Figure 3.3: A schematic illustration of the correspondence between the concentration functions given by Eq. (3.19) and Eq. (3.20) and the distribution of component A on the surface of a vesicle. ϕ_1^A and ϕ_2^A denote the regions rich and pure in component A respectively. The colour of the vesicle surface reflects the values of the local concentration of component A according to the colourmap: the blue (red) colour denotes the local concentration of component B (A), which is equal unity, and the red (blue) colour denotes the local concentration of component A (B), which is equal zero.

In our work we use the following color code to show the distribution of the components on the vesicle surface. The color of the vesicle surface reflects the local concentration values according to a given colormap. In particular, the blue (red) colour denotes the local concentration of component B (A), which is equal unity, and the red (blue) colour denotes the local concentration of component A (B), which is equal zero. Green colour denotes the total mixing of components A and B. The illustration of the local concentration profiles and the vesicles shapes are shown in Fig. 3.3. In Fig. 3.3, possible shapes of the local concentration functions are presented: (a) for both models of the concentration functions ϕ' and ϕ'', (b) only for ϕ''.

Results

CHAPTER 4

Predictions of spontaneous curvature model

4.1 One-component membrane system

Multicomponent membranes with a uniform distribution of membrane constituents can be treated as one-component membrane systems, characterized by some effective spontaneous curvature. Therefore, the analysis of the shape transformations of one-component closed vesicles with spherical topology can be considered as a first step in present studies.

Since the multicomponent membrane system is reduced to single-component one, the membrane free energy (see Section 3.4) becomes $F_{tot} = F_b$. Moreover, this assumption is equivalent to setting the local concentration function to constant (see Section 3.5) and, as a consequence, the membrane spontaneous curvature $C_0(\phi) = C_0 = constant$.

According to definition and notation of the bending energy given in Sections 2.1 and 3.3, the Hamiltonian for one-component membrane takes the form

$$\mathcal{H}(s) = \frac{\kappa}{2}(C_1(s) + C_2(s) - C_0)^2. \tag{4.1}$$

The results of minimization of the membrane free energy functional (Eq. (3.14)) with the Hamiltonian given by Eq. (4.1) and zero spontaneous curvature $C_0 = 0$ agrees very well with the phase diagram previously obtained by Seifert et al. [72]. Fig. 4.1 show three classes of vesicle shapes: stomatocyte, oblate and prolate obtained for spontaneous curvature $C_0 = 0$.

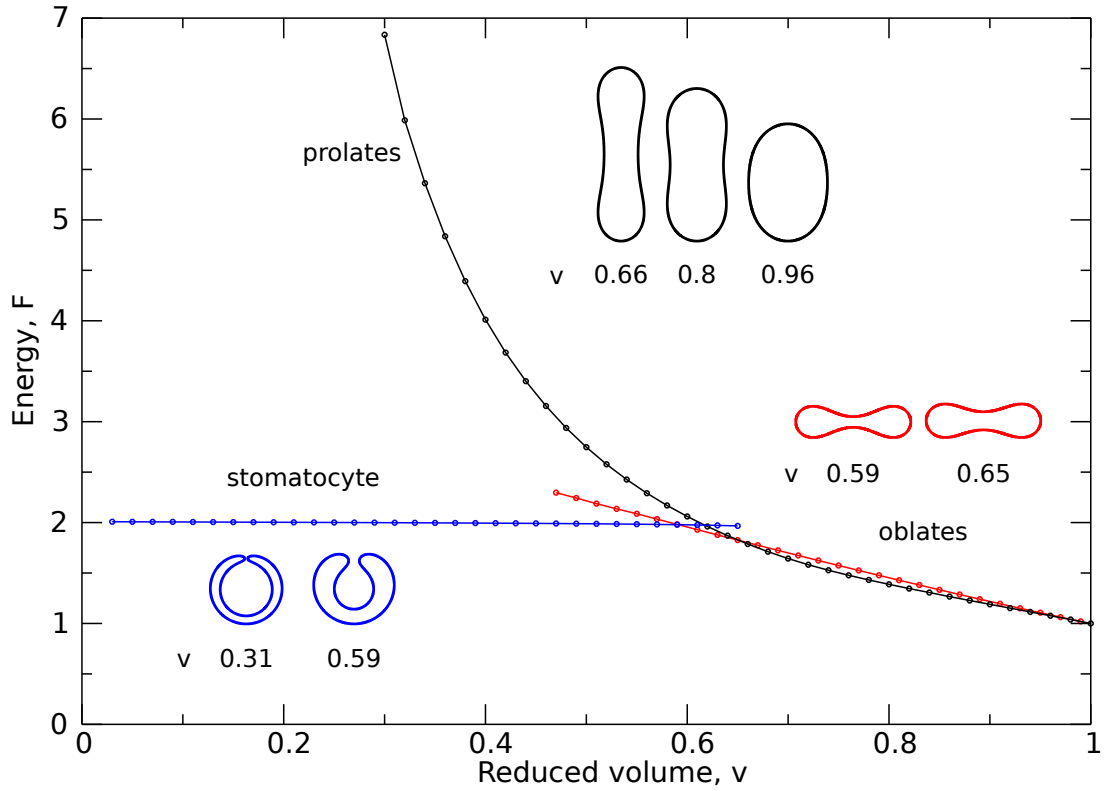

Figure 4.1: Bending energy of one-component closed vesicles for $C_0 = 0$ as a function of reduced volume v consists of three branches, which corresponds to stomatocyte (blue), prolate (black) and oblate (red) vesicle shapes. Vesicle profiles for each branch are shown for given reduced volume v. Energy is given in units $F = F_{tot}/(8\pi\kappa)$.

The results presented in Ref. [72] were performed for small values of spontaneous curvature, $0 < C_0 \leq 3$. We extended the calculation done by Seifert *et al.* to higher values of the spontaneous curvature in order to use them as a reference point for the studies of two component vesicles.

In this work we focus on vesicles with *prolate* shapes. The interest in such studies was stimulated by two reasons. Firstly, they are the most common shapes experimentally observed in both artificial and cellular membrane vesicles. Secondly, the *oblate* and *stomatocyte* vesicles are usually characterized by larger bending energy than the prolate one, is the spontaneous curvature is larger then zero, $C_0 > 0$. The prolate vesicles characterized by the lowest bending energy correspond to the stable state.

One of the examples of performed calculations is depicted in Fig. 4.2, which shows the bending energy as a function of the reduced volume and the corresponding classes

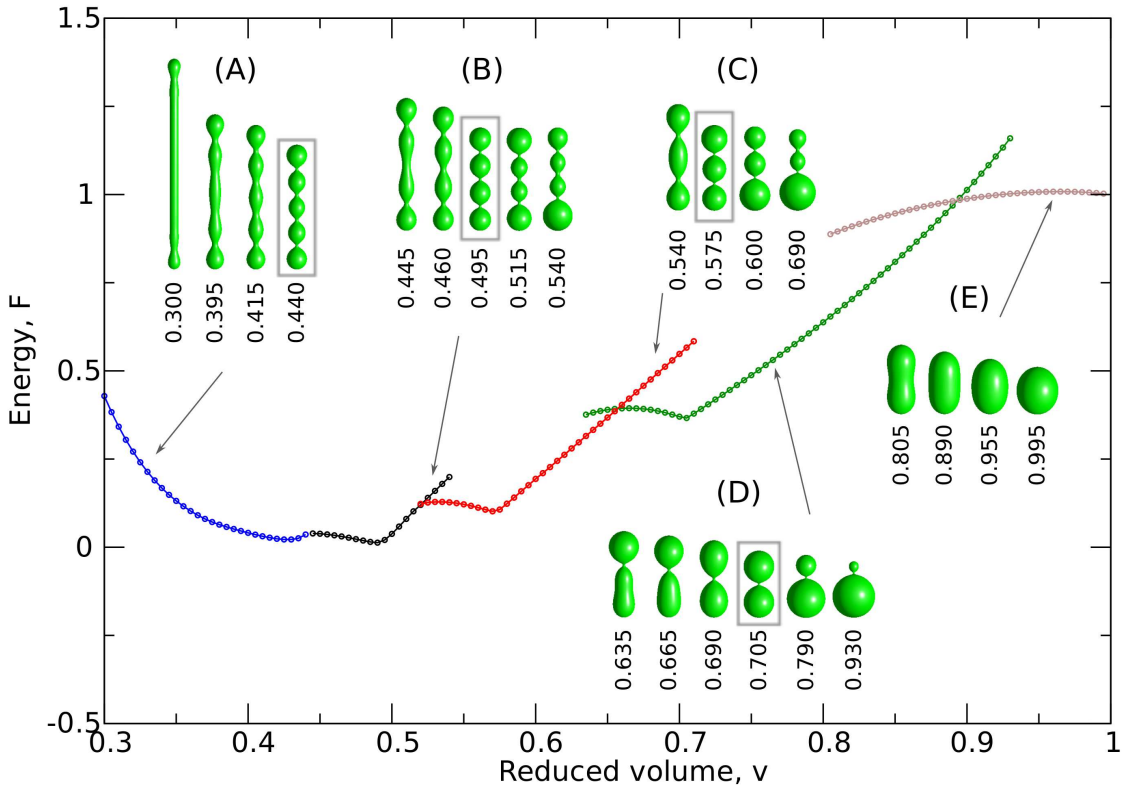

Figure 4.2: Bending energy for one-component closed axisymmetric vesicles with spontaneous curvature $C_0 = 4$ as a function of reduced volume, v. Characteristic vesicle shapes for the given value of v (number below the vesicle shape) with five (A), four (B), three (C), two (D) and one (E) beads are shown for different parts of bending energy plot. The shapes within the gray frame corresponds to local minima on the bending energy. Energy is given in units $F = F_{tot}/(8\pi\kappa)$.

of shapes for the one component vesicles characterized by the spontaneous curvatures $C_0 = 4$. It is clearly seen in Fig. 4.2 that the vesicle shapes with the spontaneous curvature $C_0 = 4$ are more structured than the vesicle shapes in Fig. 4.1 calculated for $C_0 = 0$. Therefore, one may expect that the process of separation of components due to the geometry of the vesicles can be studied effectively for the components characterized by the spontaneous curvature significantly larger then $C_0 = 4$.

4.2 Two-component membrane system

Redistribution of components on the surface of the biological multicomponent membranes is possible not only with the change of the temperature, but also with the change of the surface geometry of membrane. It is important to note that there

is a feedback between the change of membrane geometry and the distribution of components on the membrane surface, i.e. the distribution of components influences locally the surface geometry, but also the geometry of the surface may induce the component migration to the region with favorable curvature.

It is assumed, that the model membrane is composed of isotropic components A and B, characterized by spontaneous curvatures C_0^A and C_0^B. The free energy functional is given by $F_{tot} = F_b + F_{mix}$, where F_b is described by the Helfrich Hamiltonian:

$$\mathcal{H}(s) = \frac{1}{2}\kappa(\phi(s))(C_1(s) + C_2(s) - C_0(\phi(s)))^2 \tag{4.2}$$

and F_{mix} is given by Eq. 3.18. $\kappa(\phi(s))$ and $C_0(\phi(s))$ are the local bending rigidity and local spontaneous curvature, respectively, which depends *linearly* on the concentration of component A

$$C_0(\phi(s)) = (C_0^A - C_0^B)\phi(s) + C_0^B. \tag{4.3}$$

and

$$\kappa(\phi(s)) = (\kappa^A - \kappa^B)\phi(s) + \kappa^B. \tag{4.4}$$

The concentration function takes the form given by the Eqs. 3.19 or 3.20.

The bending energy functional with $C_0(\phi)$ was first introduced in work [71], where only stiff membrane was studied, *e.g.* $\kappa \gg k_BTR^2/a_0$, where R is the radius of investigated vesicle. Here we focus on a stiff as well as on a flexible membrane, $\kappa \sim k_BTR^2/a_0$, for which the entropy contribution cannot be neglected. ϕ_A, ϕ_B, ξ, and s_0 are calculated in the minimization process [73].

4.2.1 Results

The calculations were performed for $\phi_{tot} = 0.5$, and for different values of the reduced volume. The spontaneous curvatures in most cases were $C_0^A = 8$ and $C_0^B = 0$, and for a comparison also $C_0^A = 2, 4, 6$ were considered. The values of the elastic constants in most cases were $\kappa^A = \kappa^B = 30k_BT$. We have also considered $\kappa^A = 2\kappa^B$, $\kappa^A = 8\kappa^B$ and $\kappa^B = 8\kappa^A$ to determine the effect of a difference between the elastic constants of the two components. The most important factors determining the equilibrium shape of the vesicle are v and C_0^A. The minimization of the functional gives nonuniform distribution of the components, except for a few distinct cases where the distribution is uniform. For the configurations where the functional has the minimum for the uniform distribution we obtain the shape of the vesicles with up-down symmetry. The shape of

the vesicles with uniform distribution of components can be described as a sphere or beads of similar size connected by narrow passages.

The vesicles with nonuniform distribution of components do not have up-down symmetry. They are composed of a large, approximately spherical part, connected with a protrusion formed of small beads or of a cylindrical shape. For the reduced volume close to $v = 1$ the formation of long protrusions is prohibited by the volume constraint. When the reduced volume is smaller than $v = 0.95$, the vesicle is deformed and a spherical bud is formed. For decreasing v the length of the protrusion increases. The curvature of the membrane in the protrusion is larger than the local curvature in the remaining spherical part. Such shape asymmetry favors separation of the components. The concentration in the protrusion depends on v, on the parameter $k_B T R^2/\kappa a_0$, and on the way the shape deformation is induced.

Detailed results are presented in the following subsections.

4.2.2 Separation of components on a stiff membrane.

We first describe results obtained for a very stiff membrane, where the entropy of mixing can be neglected. With neglected entropy of mixing we determine the configurations of vesicles with minimized elastic energy. These results show the limits of the shape-induced segregation of the membrane components, and are analogous to the analysis of the ground state in statistical-mechanical description of ordering. Once the relation between the shape of the vesicle and the segregation of the components is established, we will be able to identify the effect of entropy on both the segregation and the shape of the vesicle. Fig. 4.3 shows comparison of the free energy for nonuniform distribution of components (solid curves) with the free energy calculated with the constraint of uniform distribution (dashed curves) when the bending rigidity is the same for both components.

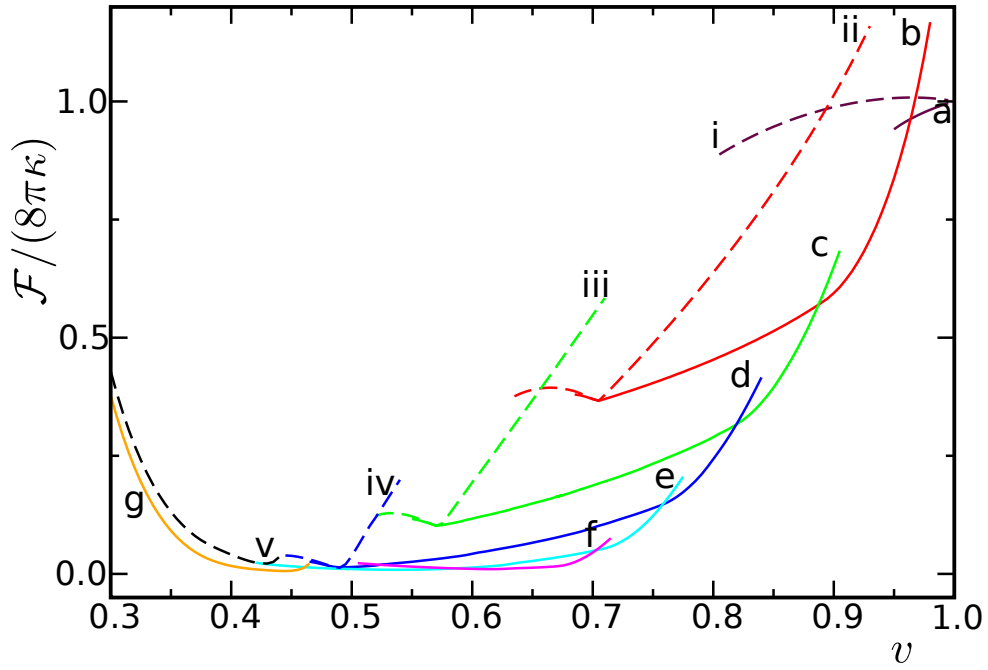

Figure 4.3: The free energy as a function of the reduced volume v. The dashed lines show the free energy obtained for constant spontaneous curvature $C_0 = 4$ (uniform distribution of components) for the following configurations: (i) a sphere, (ii) two, (iii) three, (iv) four, and (v) five beads respectively. The solid curves show the free energy for (a) partially budded configurations and configurations with: (b) one, (c) two, (d) three, (e) four, (f) five small beads, and for tubular shapes (g). The total concentration is $\phi_{tot} = 0.5$, $C_0^A = 8$, $C_0^B = 0$, $\kappa^A = \kappa^B$. Configurations corresponding to the lowest value of the free energy for given v are thermodynamically stable, the remaining ones are metastable.

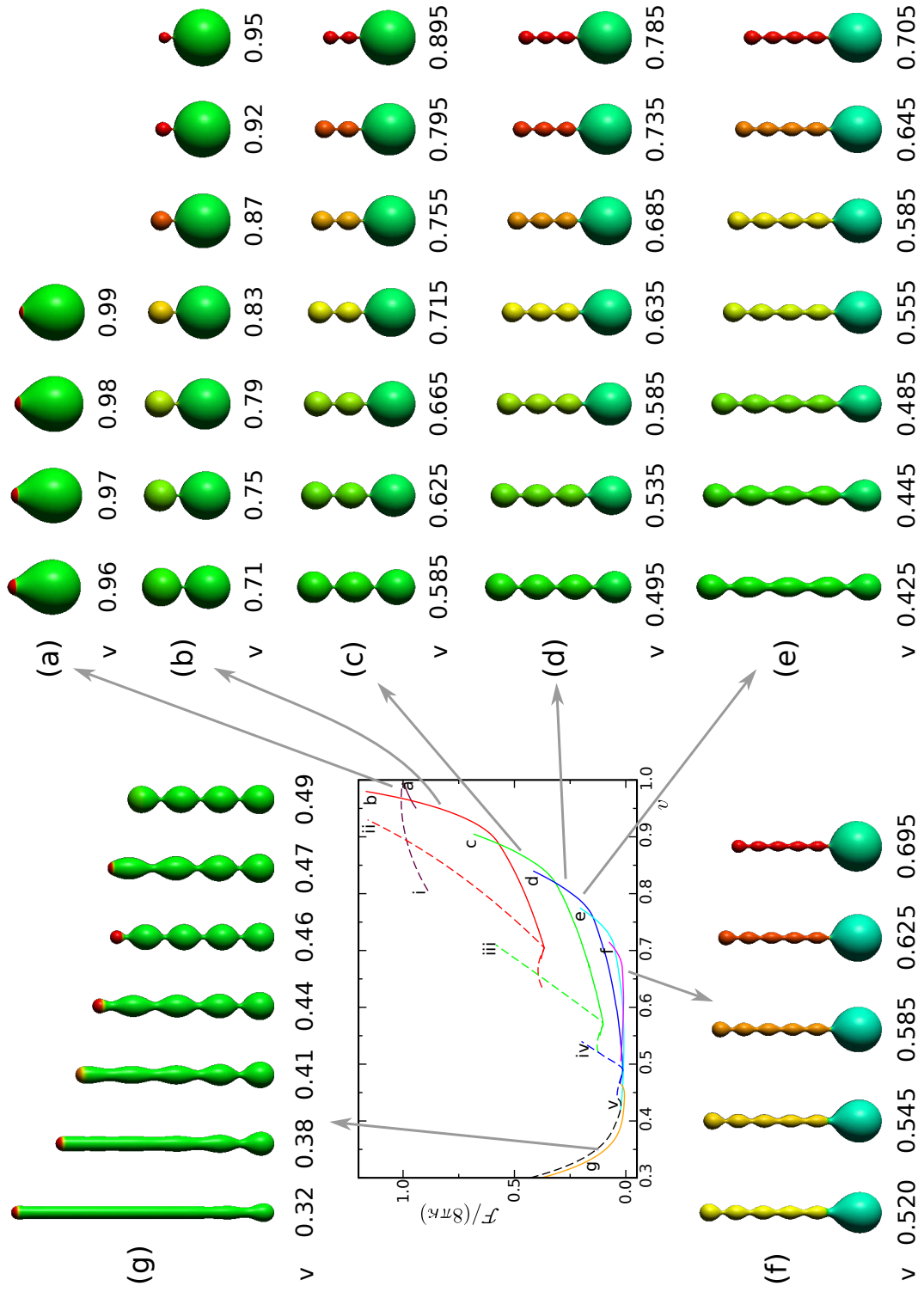

Figure 4.4: Shapes transformations of two-component vesicles corresponding to brunches of free energy function, presented on Fig. 4.3. The configurations with protrusions consisting of one (a) bead, two (b), three (c), four (d) and five (e) beads and of tubular shapes (g) are shown.

Each curve shows the free energy for a given configuration of the vesicle within the range of the reduced volume for which a stable or metastable solution is found. Outside that reduced volume range no stable solution for a given configuration has been obtained. These curves have a few common parts which mark the configurations where the minimum of the functional is obtained for uniformly mixed components.

In a similar way the free energy was analysed with the entropy contribution included. The shape transformations induced by the change of the reduced volume v are shown in Fig. 4.4.

The concentration of the component with larger spontaneous curvature in the bud is much higher than in the remaining spherical part of the vesicle, where the components are almost equally mixed.

The configurations with the spherical bud are stable (metastable) for the reduced volume $0.88 < v < 0.96$ ($0.7 < v < 0.88$). The first vesicle on the left (b,c,d,e) in Fig. 4.4 represents the uniform distribution of the components for the configuration with two beads. The following vesicles represent the change of the shape and distribution of the components with increasing reduced volume. The increase of the reduced volume with given number of beads leads to demixing. The size of the upper bead rich in the component A is coupled to the concentration in that bead. This can be easily understood since the spontaneous curvature depends on concentration. The larger is the concentration ϕ of the component with $C_0^A = 8$, the larger spontaneous curvature $C_0(\phi)$ is induced, and the smaller is the size of the bead.

In Fig. 4.4 the configurations with protrusions consisting of one bead, two , three , four and five beads and of tubular shapes (g) are shown. The shapes with protrusions

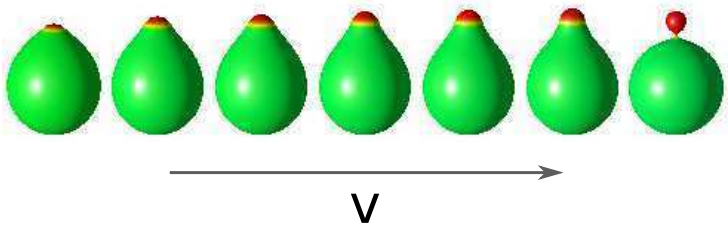

Figure 4.5: Budding of two-component vesicle induced by the change of the reduced volume v. From the right to the left vesicle $v = 0.94, 0.95, 0.955, 0.96, 0.97, 0.975, 0.99$ respectively. The arrow indicates the direction of decreasing of v. The total concentration is $\phi_{tot} = 0.5$, $C_0^A = 8$, $C_0^B = 0$, $\kappa^A = \kappa^B$.

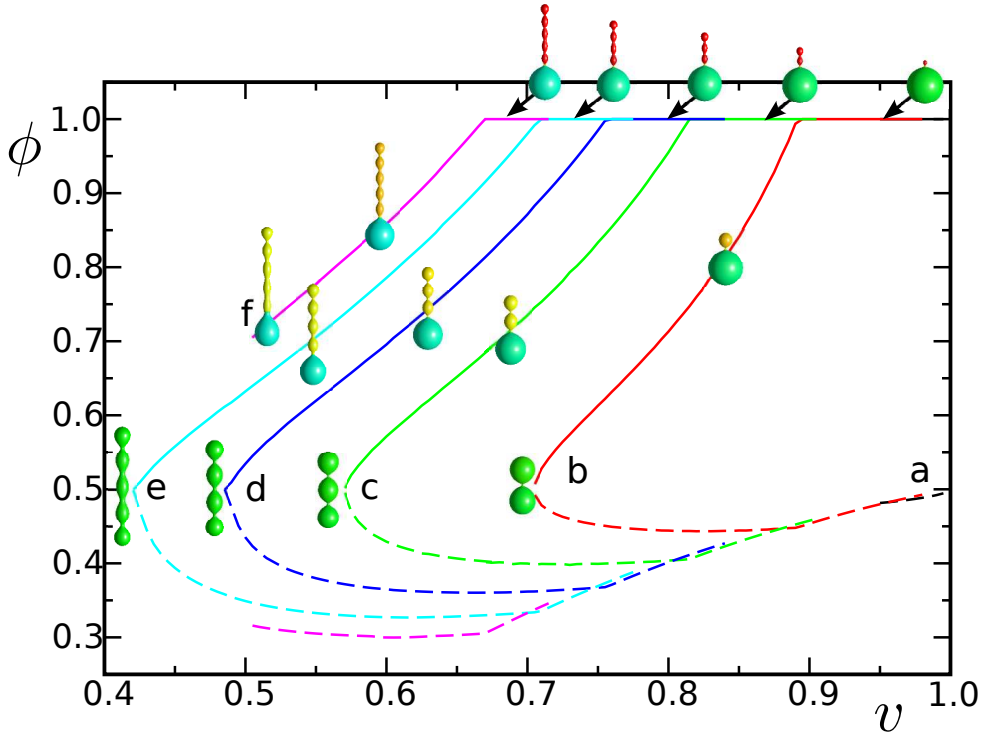

Figure 4.6: Concentration of component A in the spherical part of the vesicle (dashed curves) and in the protrusion (solid curves) as a function of the reduced volume v for different shapes of vesicles for (a) configurations without the beads, and configurations with: (b) one, (c) two, (d) three, (e) four, (f) five small beads. The total concentration is $\phi_{tot} = 0.5$, $C_0^A = 8$, $C_0^B = 0$, $\kappa^A = \kappa^B$.

consisting of two or four beads are similar to the shapes of three-bead protrusions, with one less or one more bead respectively. When the reduced volume v decreases, the number of beads in the protrusion increases until $v < 0.4$ where tubular shapes become stable. For small values of the reduced volume the vesicle is occupied by almost totally mixed components, except for a small region at the pole of the vesicle, where the concentration of the component characterized by large spontaneous curvature is high (see Fig. 4.4).

The calculated two-bead shapes might be linked with the process of budding of the vesicle induced by the decreasing of reduced volume (see Fig. 4.5).

In Fig. 4.6, the curve (a) shows the concentration in the partial bud, and the curves (b, c, d, e, f) represent the concentration in the protrusions composed of one, two, three, four, and five small beads respectively (solid curves) and in the remaining part of the vesicle (dashed curves). In several cases the protrusion is occupied mainly by the component with large spontaneous curvature. The largest concentration difference

can be obtained for the configurations with five small beads, when the protrusion is occupied almost exclusively by the component with $C_0^A = 8$. In most cases the component A is mixed with the component B in the spherical part of the vesicle, because the surface area of the protrusion is too small, and some amount of the component A is left even when its concentration in the protrusion is close to $\phi = 1$.

We have also investigated the separation for smaller values of the spontaneous curvature $C_0^A = 2, 4, 6$ and $C_0^B = 0$. For $C_0^A = 2, 4$ and $C_0^B = 0$ no configuration with protrusions or buds is stable. For smaller values of the reduced volume configurations with pear-like shapes with nonuniform distribution of components are stable. The uniform distribution of components was observed only for the reduced volume $v = 1$. For $C_0^A = 6$ and $C_0^B = 0$ we have found the configurations with the protrusions composed of only one or two small beads. For such configurations the components can be mixed and demixed by changing the reduced volume. It is possible to obtain almost complete separation of components for appropriate choice of the spontaneous curvatures. For $C_0^A = 4.5$, $C_0^B = 3.5$, $\phi_{tot} = 0.5$, and $v = 0.6$ the components are separated between the protrusion composed of two beads (where the concentration of component A is close to $\phi = 1$) and the rest of the vesicle (where the concentration of component A is close to $\phi = 0$). For the configurations with three small beads such complete separation is obtained for $v = 0.55$. In the next subsections we study how the above best segregation of the components induced by optimization of the shape of the vesicle is influenced by the entropy of mixing.

4.2.3 The effect of entropy of mixing on the separation of components.

In this section we study how the segregation of the components resulting from the minimization of the elastic energy is influenced by the entropy of mixing. We shall consider two cases: (i) the elastic constants of both components are the same, and (ii) the elastic constants are different. In the latter case the stiffer component can be associated either with the larger or with the smaller spontaneous curvature.

The entropy of mixing substantially suppresses the segregation of the components due to curvature of the vesicle surface. Obviously, the role of the entropy depends on the parameter $k_B T R^2/\kappa a_0$ which at room temperature and for a given lipid depends on the size of the nanodomain - i.e. on the kind of the macromolecules and also on the

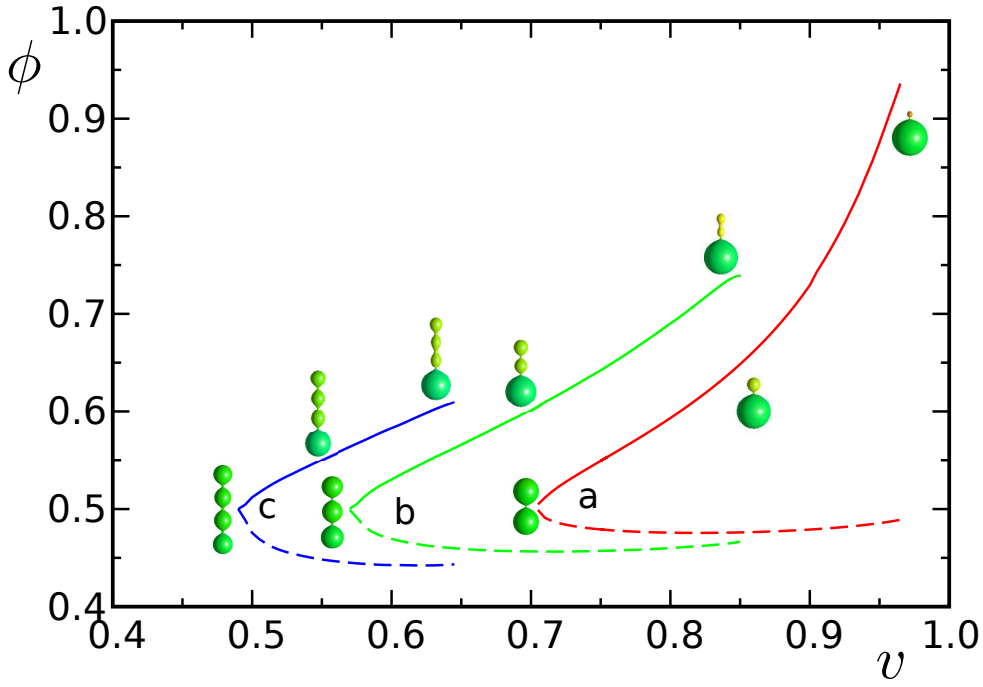

Figure 4.7: Concentration of component A in the spherical part of the vesicle (dashed curves) and in the protrusion (solid curves) as a function of the reduced volume v for the different shapes of vesicles for configurations with: (a) one, (b) two, (c) three beads. The total concentration is $\phi_{tot} = 0.5$, $C_0^A = 8$, $C_0^B = 0$, $\kappa^A = \kappa^B = 30k_bT$, $a_0 = 100nm^2$ and $R = 250nm$. The vesicle shapes represent minimized configurations with the best separation of the components (for the largest v for a given family of shapes), totally mixed (for the smallest v for a given family of shapes) , and intermediate.

size of the vesicle. Experimentally relevant cases concern R of order of $100nm - 1\mu m$ and a_0 of order of $100nm^2$. We find that the components may still segregate due to the curvature of the membrane when the domain formed by one of the components is of the order of $100nm^2$, the radius of the vesicle is of the order of $250nm$, and the bending rigidity is $\kappa = 30k_bT$. For the above parameters the configurations with the number of small beads greater than three are no longer stable. In Fig. 4.7 we present the curves which show the concentration of component A in the spherical part and in the protrusion composed of small beads as a function of the reduced volume v for three different configurations. Let us compare Figs.4.7 and 4.6 to analyse the effect of entropy on the segregation of the components. The first difference between Figs. 4.7 and 4.6 concerns the relation between the length of the protrusion and the best segregation of the components. From Fig.4.7 it follows that the excess concentration of component A in the protrusion *decreases* when the length of the protrusion increases

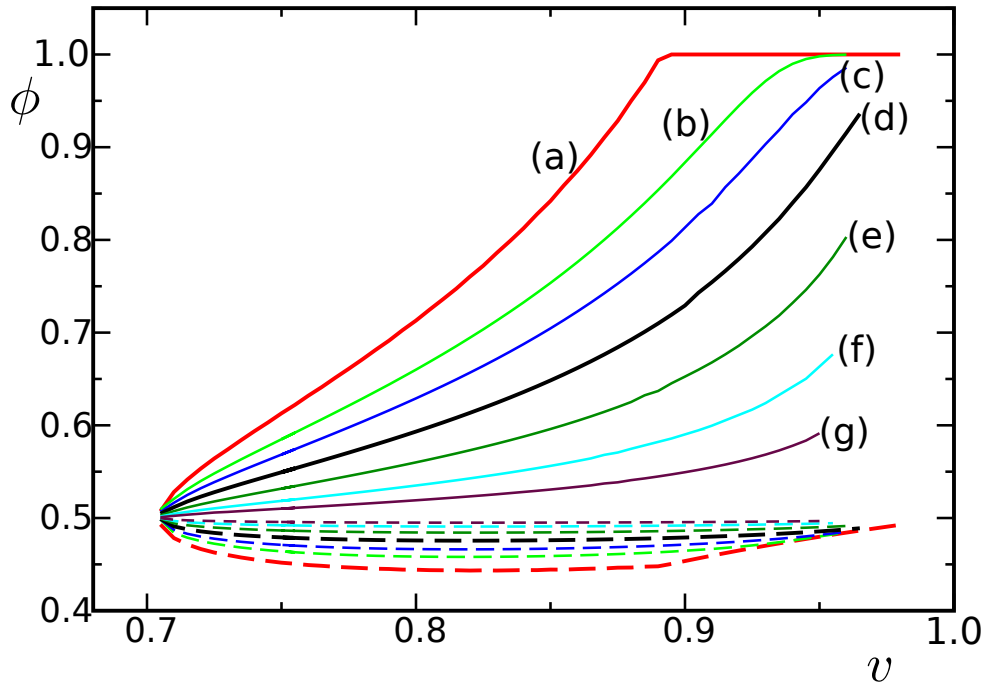

Figure 4.8: Concentration of component A in the spherical part of the vesicle (dashed curves) and in the protrusion (solid curves) as a function of the reduced volume v for configurations with one bead for different sizes of nanodomains: (b) $a_0 = 400nm^2$, (c) $a_0 = 200nm^2$, (d) $a_0 = 100nm^2$, (e) $a_0 = 50nm^2$, (f) $a_0 = 25nm^2$, (g) $a_0 = 12nm^2$. The curve (a) refers to the calculations with neglected entropy of mixing. The total concentration is $\phi_{tot} = 0.5$, $C_0^A = 8$, $C_0^B = 0$, $\kappa^A = \kappa^B = 30k_bT$, and $R = 250nm$.

- the best segregation is obtained in the case of a single bud, i.e. when the reduced volume is large. This is quite opposite to the previously studied case - in the absence of entropy the best segregation of component A in the protrusion was obtained for five beads, i.e. for much smaller v. Whereas in the absence of entropy the configurations with a protrusion consisting of a given number of beads are stable for a large range of v that increases with increasing number of beads (see Fig.4.6), in the presence of entropy the range of v for which given configuration is stable decreases for increasing number of beads, and is much smaller than in the absence of entropy (see Fig.4.7). The size asymmetry between the beads in the protrusion and in the spherical part of the vesicle increases with v for a given number of beads (see Fig. 4.4). The increase of the size asymmetry is accompanied by the segregation of the components - these two effects influence each other. In the very stiff membrane (Fig. 4.6) for each number of beads in the protrusion there exists a range of reduced volumes - the largest v for which a given number of beads is stable - for which the concentration in the protrusion

is $\phi \sim 1$. For the largest v corresponding in the absence of entropy to the stability of a given number of beads the shapes with the same number of beads are unstable in the presence of entropy. This can be easily seen by comparing the curve (d) in Fig.4.6 with the curve (c) in Fig. 4.7. Thus, the effect of entropy is to reduce segregation, and as a consequence the stability of long protrusions with very small beads that were formed in the presence of segregation. Since the segregation increases with increasing v for fixed number of beads, and range of v corresponding to a single bead is larger than in the case of two and three beads, the best segregation of the components is obtained for a single bead.

We have also examined the influence of the nanodomain size on the separation of components. The calculations were performed for a single bead, i.e. for the best segregation. The calculations for a vesicle with the radius $R = 250nm$ and a few sizes of nanodomains with surface area larger and smaller then $a_0 = 100nm^2$ are presented on Fig. 4.8. Even for very small nanodomain size $a_0 = 12nm^2$ the components separate, although very weakly. The difference of concentration is approximately 10% in the optimal case, where the bead sizes differ the most. It is interesting to note that even very weak separation of components may stabilize configurations with small beads. In all cases it was possible to obtain stable configurations with the reduced volume up to $v = 0.95$.

We have also examined the system where the components have different bending rigidity. Fig. 4.9 shows the plots of the concentration of component A in the spherical part of the vesicle and in the protrusion composed of small beads for bending rigidity $\kappa^B = 30k_bT$, $\kappa^A = 8\kappa^B$ (the left side) and $\kappa^A = 30k_bT$, $\kappa^B = 8\kappa^A$ (the right side). In both cases the dependence of the concentration in the protrusion and the spherical part of the vesicle on v is similar as in the case of equal elastic constants of the components, but higher bending rigidity of one component enhances the separation, as can be seen by comparing Figs. 4.9 and 4.7. In the case of a single bead (large v) the small bead is composed of nearly pure A component when the membrane with attached macromolecule is stiffer (Fig.4.9A).

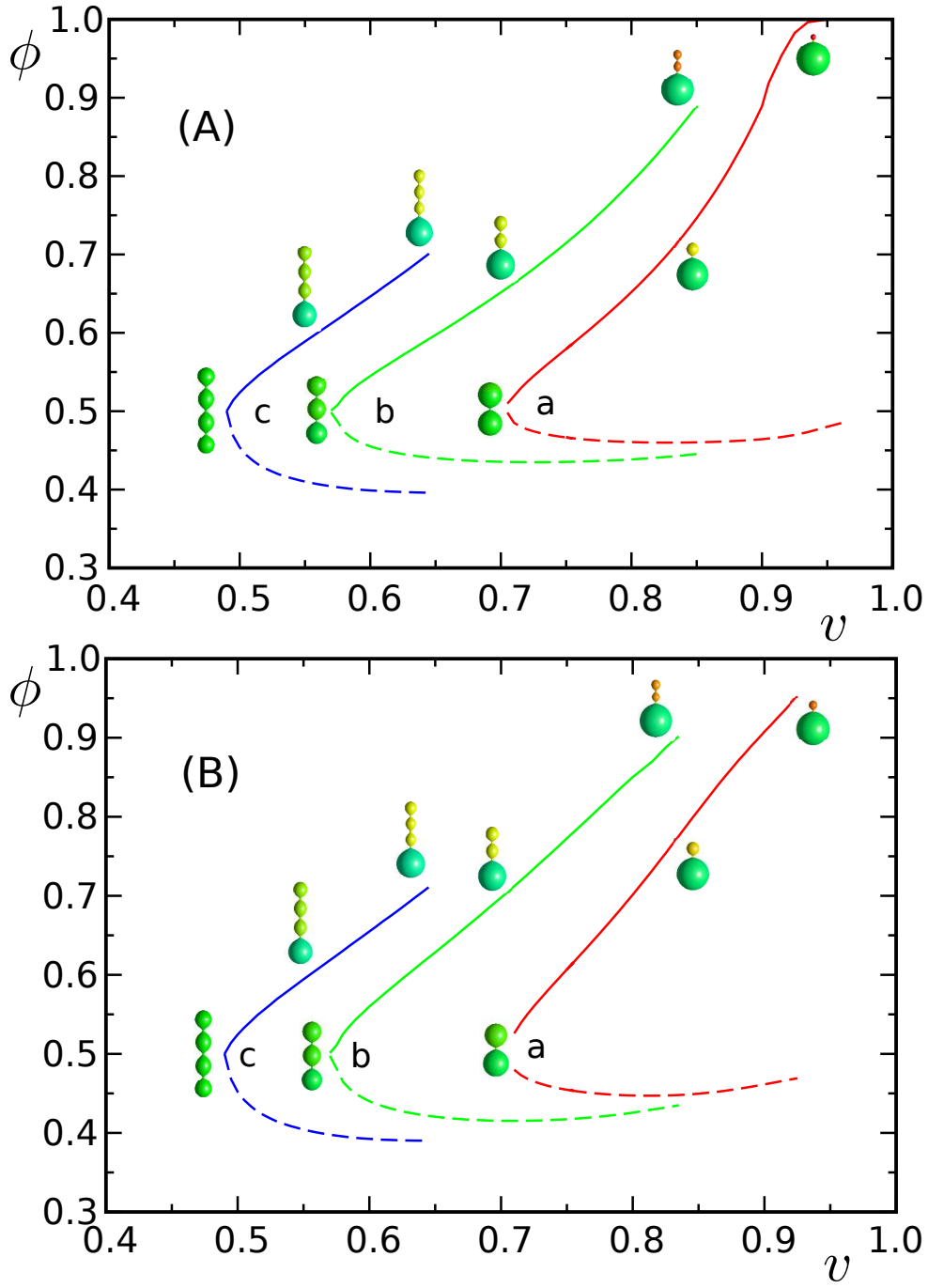

Figure 4.9: Concentration of component A in the spherical part of the vesicle (dashed curves) and in the protrusion (solid curves) as a function of the reduced volume v for the different shapes of vesicles for configurations with: (a) one, (b) two, (c) three beads:(A) $\kappa^A = 8\kappa^B, \kappa^B = 30k_bT$, (B) $\kappa^A = 30k_bT, \kappa^B = 8\kappa^A$. The total concentration is $\phi_{tot} = 0.5$, $C_0^A = 8$, $C_0^B = 0$, $a_0 = 100nm^2$ and $R = 250nm$. The vesicle shapes represent minimized configurations with the best separation of components (for the largest v for a given family of shapes), totally mixed (for the smallest v for a given family of shapes), and intermediate.

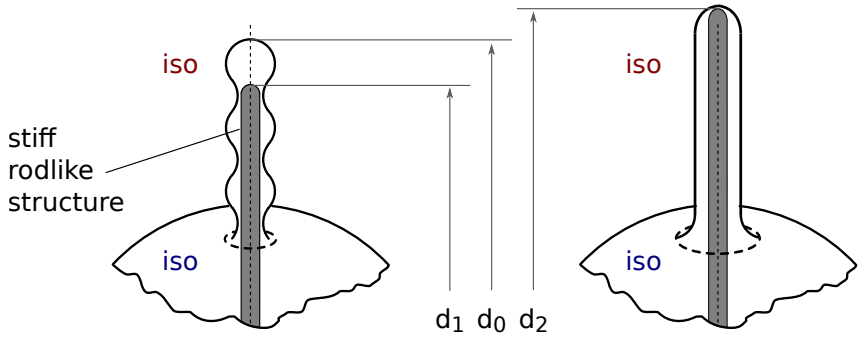

Figure 4.10: Schematic representation of a vesicle profile with a growing microtubule inside. d_1 is the length of the microtubule in comparison with the length of the membrane protrusion d_0 before "pulling". d_2 is the length of the membrane protrusion pulled out by microtubule, which is equal to the length of microtubule.

4.2.4 Separation of components induced by elongation of the vesicle

For the sake of simplicity let us focus on the case when the application of external force is understood as a presence of stiff microtubule inside the vesicle, see Fig. 4.10. It is assumed that microtubule is rigid and located inside a vesicle along its axis of rotation.

The minimization of Eq. 4.2 is performed with additional constraint on the distance between the ends of the vesicle, which corresponds to a given length of the microtubule. It is assumed that the growth of a microtubule is slower than the shape relaxation of the vesicle.

The change of the vesicle volume is not the only or the most convenient way to change the shape of the vesicle. In experiments it might be easier to change vesicle shape by elongating it [74,75]. A vesicle may be elongated from outside by pulling the membrane by laser tweezers or from inside by growing microtubules [76]. The external force applied to the poles of the vesicle can keep them at fixed separation, without changing the area of the membrane. In mechanical equilibrium the external force is compensated by the elastic force resulting from deformation of the vesicle shape. Such systems are modeled in our analysis by imposing a constraint on a distance between the poles of a vesicle [77], in addition to the constraints of fixed area and volume. When a vesicle is elongated, a cylindrical protrusion is formed at its nearly spherical surface, see Fig. 4.11. Thus, the vesicle is composed of two parts with different mean curvatures. Such difference of the mean curvatures may be the driving force for

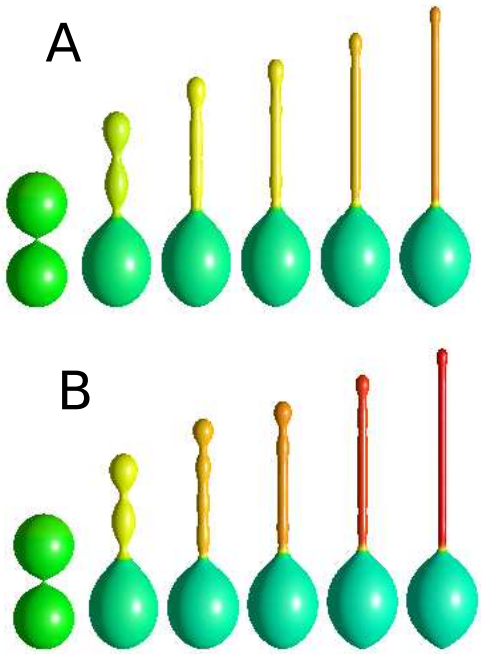

Figure 4.11: The shapes of vesicles with lateral segregation induced by elongation: (A) $\kappa^A = 2\kappa^B, \kappa^B = 30k_bT$, (B) $\kappa^A = 8\kappa^B, \kappa^B = 30k_bT$. The total concentration is $\phi_{tot} = 0.5$, $C_0^A = 8$, $C_0^B = 0$, $a_0 = 100nm^2$ and $R = 250nm$. The height of the vesicle $H = 3.1, 4.5, 5.3, 5.7, 6.3, 6.9$ in R units. The reduced volume $v = 0.705$.

segregation of the components with different spontaneous curvatures.

Note that in the previously studied example the segregation and shape transformations influenced each other as a result of the competition between the elastic energy and the entropy of mixing. When the segregation was suppressed by the entropy, then the long protrusions could not be formed. In this case the external force that keeps the poles of the vesicle at the prescribed distance induces the formation of the protrusion that favors the segregation of the components. The entropy of mixing and the elastic energy can influence the shape of the vesicle without the change of the distance between the poles.

In Fig. 4.11 we present the results of the calculations performed for two systems, where the components differ by the spontaneous curvature and the bending rigidity. The component with larger spontaneous curvature is characterized by the bending rigidity two (Fig. 4.11A) and eight (Fig. 4.11B) times larger than the component characterized by smaller spontaneous curvature. Fig. 4.11 shows shapes of vesicles minimized for a few values of the distance between the poles. In the first configuration

the components are completely mixed, $\phi = 0.5$ at every point of the surface and no external force is applied to the poles of the vesicle. The next configurations show elongated vesicles minimized with the constraint of a fixed distance between the poles. Increasing the bending rigidity of the component characterized by larger spontaneous curvature enhances the separation. It is interesting to note that the length of the cylindrical protrusion is correlated with the concentration of components in the protrusion. Longer protrusions have higher concentration of the component characterized by the larger spontaneous curvature. Longer protrusions are also thinner, therefore the mean curvature of the cylindrical protrusion is larger. Thus, the difference of the curvature between longer cylindrical protrusion and the spherical part of the vesicle is larger which creates the driving force for curvature driven segregation of components [78]. The process described above should be reversible, when the distance between the poles of the vesicle is no longer constrained the vesicle should return to its original state where the components are totally mixed.

4.2.5 Conclusions

It has been shown that the separation of membrane components in a bilayer vesicles can be induced by the change of the vesicle shape in a similar way as it is usually done by the change of temperature [79]. The separation of membrane components may occur, however, only for a certain range of parameter values, *e.g.* the size of the vesicle, area occupied by the macromolecules attached to one of the components in the outer monolayer, spontaneous curvatures, and elastic moduli of the components. Elongation of a vesicle or changing its volume induces the change of a vesicle shape in such a way that in thermodynamic equilibrium the component characterized by large spontaneous curvature accumulates in the region with large local curvature, and thus is separated from the other component. The separation, however, is incomplete and occurs only for rather narrow range of the reduced volume. In future experiments the reduced volume should be carefully tuned to observe the lateral separation of membrane components. In biological systems the volume of the cell vesicle can be altered when the osmotic pressure is changed. When the volume is changed, the components start to migrate to regions with local curvature that matches better their spontaneous curvature, and simultaneously with the migration (and hence the change

of the local concentration) the local curvature is changed. This mechanism is effective only for large macromolecules in the membrane, with linear extension $\gtrsim 0.01R$. The area of the bead with high concentration of A component is rather small, but it can be enlarged at the cost of weaker segregation (Fig. 4.4), still much more effective than found for two types of lipids [80].

Important result of our work is the observation that elongation of a vesicle may lead to formation of tubular protrusions occupied mainly by a component with larger spontaneous curvature. For long protrusions stretching a vesicle can be an efficient segregation mechanism of the component with significantly larger curvature, provided that the area occupied by the attached molecules inducing the large curvature is sufficiently large.

CHAPTER 5

Predictions of deviatoric elasticity model

This Chapter is devoted to the question of the formation and stabilization of the tubular membrane structures (protrusions and connecting (nano)tubes) caused by the presence of anisotropic membrane constituents coupled with their lateral (re)distribution in the membrane.

Intrinsic curvature mechanism (*i.e.* the intrinsic shapes of membrane components) of component segregation may be especially important in the process of formation of membrane tubular structures (Fig. 5.1). It was shown in a number of theoretical and experimental studies, that generation and stability of the membrane tubular structures in the cellular and artificial multicomponet membrane systems in the absence of any intercellular rigid structures, *e.g.* microtubules, or external pulling forces, such as optical tweezers or motor proteins (kinesin, dynamin) is possible and can be explained by *the accumulation of anisotropic membrane components in the tube region* [81–84]. In the case, when the external pulling/pushing force is present the accumulation of membrane components in the favorable curvature regions facilitates the tube growing process and stabilizes its final equilibrium shape.

As it was mentioned in Section 2.2, that the concept of *anisotropy* of membrane constituents is crucial for understanding the mechanisms inducing the formation of tubular membrane structures observed in both cellular and artificial biomembrane

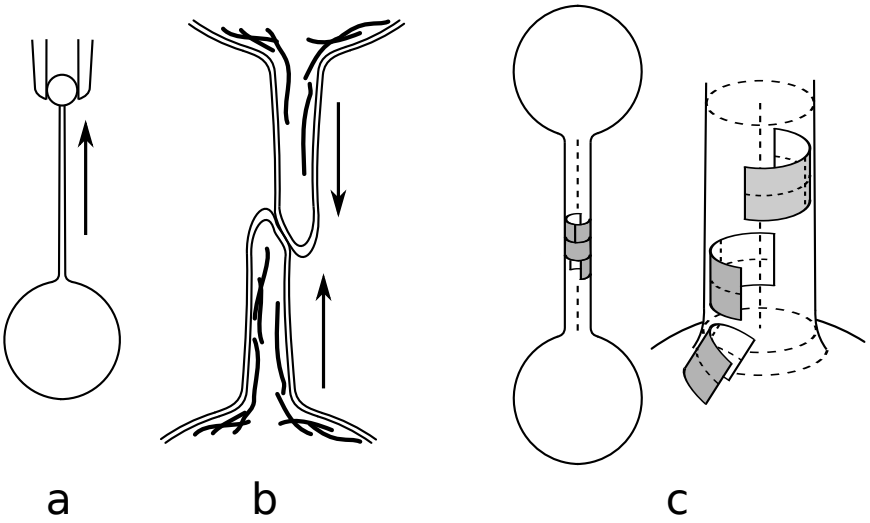

Figure 5.1: Mechanisms of formation of membrane tubular structures. The formation of tubular structure with application of external pulling force, *e.g.* (a) pulling membrane from outside by micropipette, (b) pulling membrane from inside by elements of cell cytoskeleton. The examples of formation of tubular structure without application of external pulling force is shown in scheme (c).

systems[1].

According to the *spontaneous curvature model* (see Section 2.1) of membrane elasticity, long membrane protrusions cannot be fully stabilized by membrane components with rotational symmetry (*isotropic*) without application of some additional external force. Theoretically this process can be investigated within the framework of the *deviatoric elasticity model* (see Section 2.2), the generalized form of SC model, where the membrane components are considered as *anisotropic*, whereas in the limiting case (see Subsection 2.2.2) components can be isotropic as it is assumed in SC model), *i.e.* do not have a rotational symmetry.

[1]It was experimentally observed that adding a dimeric cationic amphiphiphile molecules to the erythrocyte suspension results in a release of a stable tubular structures from the erythrocyte membrane, [85].

Another experimental example is related to the stability of tubular membrane protrusions. Fibroblast cells treated with cytochalasin B produce long membrane protrusions with rod-like microtubules inside. Whereas, the same treatment of cells with reduced content of cholesterol in the membrane results in thinner and smoother tubular membrane protrusions without the microtubules inside [86].

5.1 Two-component membrane system without the application of external pulling force

It is assumed, that the model membrane is composed of components A and B which can be either *isotropic* or *anisotropic* and are characterized by intrinsic principal curvatures C^i_{1m}, C^i_{2m} ($i =$ A, B). The free energy functional is composed of the (anisotropic) bending energy F_b and the free energy associated with the entropy of mixing F_{mix}, given by Eq. (3.18), $F_{tot} = F_b + F_{mix}$.

As it is clearly seen from Eq. (2.7) the elastic energy per nanodomain directly depends on its orientation, therefore, for the simplest case ($\omega = 0$), used in the present implementation, the membrane bending energy takes the form [66]:

$$F_b = \int_A \kappa(\phi) \left[(H - H_m(\phi))^2 + (D - D_m(\phi))^2 \right] dS. \tag{5.1}$$

Note, that a membrane component is considered as isotropic when its intrinsic deviatoric curvature is zero, $D^i_m = 0$ ($C^i_{1m} = C^i_{2m}$). The properties of anisotropic membrane components are defined by setting $D^i_m \neq 0$,. In particular case corresponding the *cylindrical* shape of membrane nanodomain (see Fig. 1.4 (d)), intrinsic devatoric and mean curvatures are set equal, $D^i_m = H^i_m$.

For simplicity we assume *linear* dependence of bending rigidity κ, nanodomain intrinsic mean curvature H_m and deviator D_m on relative concentration of the component A, ϕ :

$$\kappa(\phi) = (\kappa^A - \kappa^B)\phi + \kappa^B \ , \tag{5.2}$$

$$H_m(\phi) = (H^A_m - H^B_m)\phi + H^B_m \ , \tag{5.3}$$

$$D_m(\phi) = (D^A_m - D^B_m)\phi + D^B_m \ , \tag{5.4}$$

where κ^A and κ^B are bending rigidities of components A and B, respectively. The ansatz for the local relative concentration of the component A, $\phi = \phi(s)$, is given by of Eq. (3.20).

5.1.1 Results

Here the special attention is devoted to the stability and growth of tubular membrane structures with thin tubular protrusions, with and without the small spherical vesicles

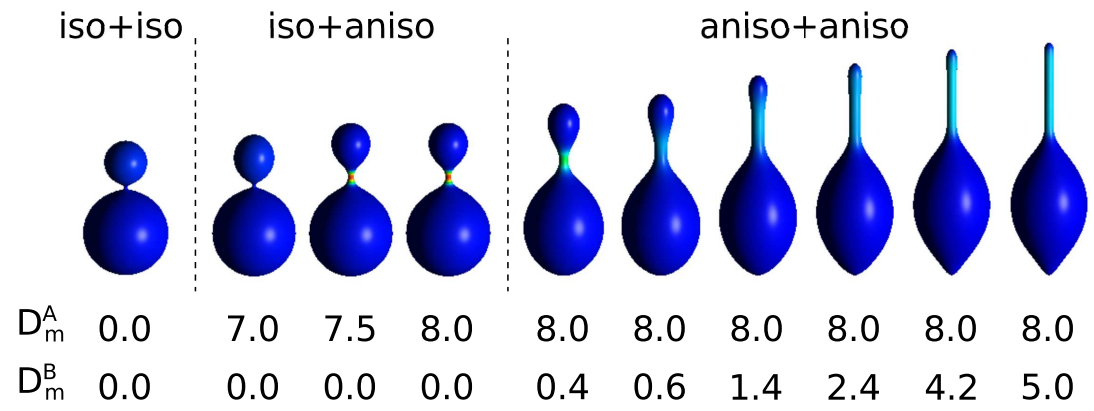

Figure 5.2: The shapes of the vesicle composed of both isotropic (iso+iso), mixed (iso+aniso) and both anisotropic (aniso+aniso) components for vesicle shapes for different concentration, ϕ, of anisotropic component for $v = 0.8$, $\phi = 0.02$, $H^A_m = 8.0$, $H^B_m = 4.2$, $\kappa^A = 4\kappa^B$ ($\kappa^B = 30 k_B T$).

at their free tips, induced by accumulation of anisotropic membrane components in tubular membrane regions *without* the application of the external force [87–89].

The results have shown that *cylindrical protrusions* are formed when at least one of the membrane component is characterized by rather high anisotropy.

Fig. 5.2 shows the shape transformation of the vesicle induced by the change of intrinsic geometry of one of the membrane constituents. For the case, when both components are *isotropic*, the vesicle is composed of small spherical beads connected by narrow passages [2]. The change of the intrinsic geometry of one of the components by setting the value of the intrinsic deviatoric curvature different form zero, $D^A_m \neq 0$, results in a shape change of the vesicle and the formation of tubular structure (Fig. 5.2). Note, that the shape of the vesicle became elongated when both components are anisotropic ($D^A_m \neq 0$, $D^B_m \neq 0$). Similar shapes are observed for vesicles with both isotropic components when the external pulling/pushing force is applied.

So far, the formation of thin cylindrical protrusions attached to larger spherical vesicle has not been shown in the models in which the anisotropy of the components is not taken into account. It was observed [87], that tubular membrane structures might be formed even for a very small amount of an anisortopic component present in the membrane, however, again, the latter has to be characterized by rather *high* intrinsic curvature. Such behavior is demonstrated in Fig. 5.3, where the concentration of anisotropic

[2]Roughly speaking, such results may be referred to those obtained by using the SC model.

component is varied from $\phi = 0.01$ to $\phi = 0.055$. Furthermore, as it is clearly seen from Fig. 5.3, the length and the radius of membrane protrusion strongly depend on the concentration of anisotropic membrane component. The anisotropic membrane component is located mainly in the tubular part, which has a very small surface area compared to the rest of the vesicle area. The *total membrane component separation* was observed for $\phi = 0.02$. At this concentration almost all anisotropic component was accumulated in the neck of the vesicle[3].

The calculations presented in Fig. 5.3 were performed for constant reduced volume $v = 0.8$. For such a reduced volume we observe the shapes without up-down symmetry, but for smaller values of the reduced volume the shapes with up-down symmetry are stable, as presented in Fig. 5.4. Moreover, the smaller the volume the more mixed are the components, and the cylindrical protrusions are no longer stable.

The total mixing was observed for small concentration of anisotropic component, $\phi = 2\%$, which for small reduced volume, $v > 0.65$, results in pearl-like shapes with up-down symmetry. The increase of the concentration of anisotropic component stabilizes longer and wider tubular structures.

The anisotropy of one of the membrane components is not however a sufficient condition for formation of the tubular membrane structures. We have also observed that cylindrical protrusions may be induced by changing the properties of the isotropic

[3]Note, that the possibility of accumulation of membrane components in a small area region might be one of the important mechanisms of activation of some important biological membrane functions like for example vesicle fusion and fission.

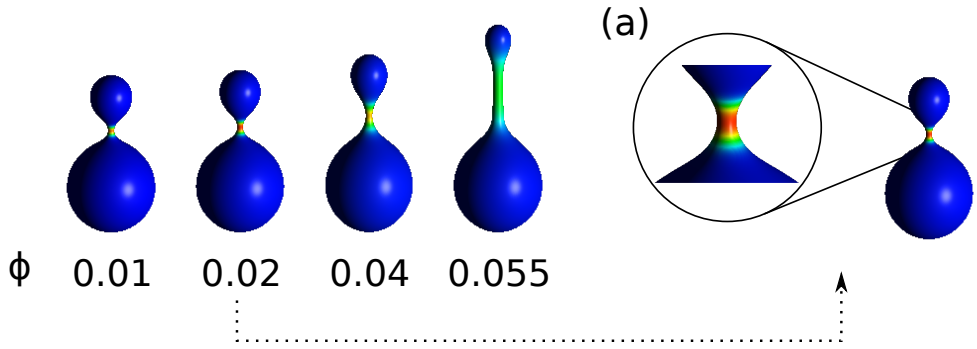

Figure 5.3: The calculated vesicle shapes for different concentration, ϕ, of anisotropic membrane component, and for $H_m^B = 4.2$, $v = 0.8$, $H_m^A = D_m^A = 8.0$, $\kappa^A = 4\kappa^B$. $\kappa^B = 30 k_B T$. The inset (a) shows the configuration with almost total segregation of membrane components for $\phi = 0.02$. The anisotropic component is accumulated in the neck area.

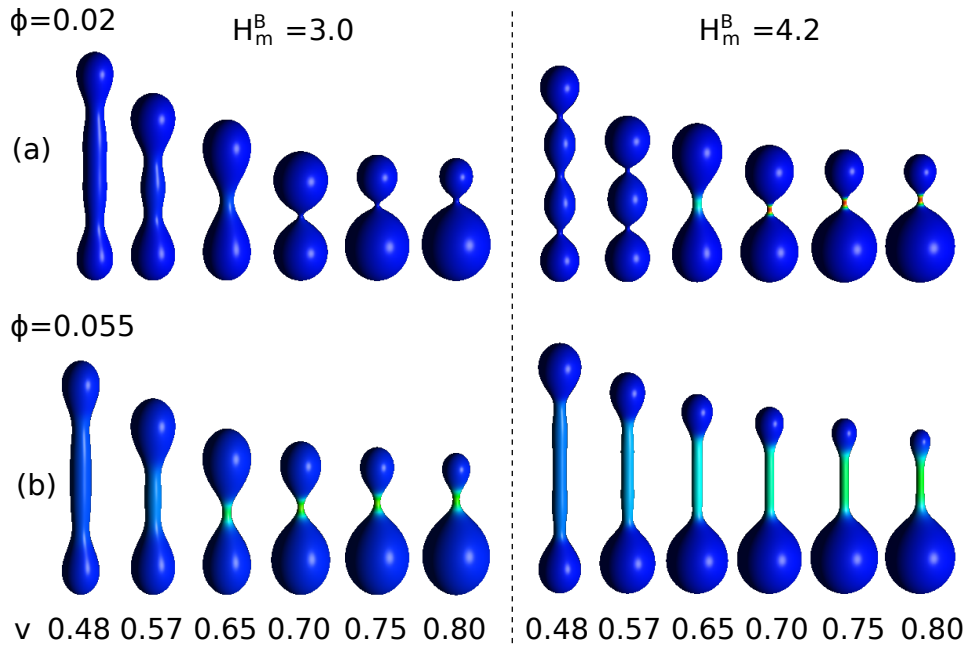

Figure 5.4: The calculated vesicle shapes for different values of the reduced volume, v, and for (a) $\phi = 0.02$, $H_m^B = 3.0$ (left), $H_m^B = 4.2$ (right), $H_m^A = D_m^A = 8.0$, $\kappa^A = 4\kappa^B$ and (b) $\phi = 0.055$, $H_m^B = 3.0$ (left), $H_m^B = 4.2$ (right), $H_m^A = D_m^A = 8.0$, $\kappa^A = 4\kappa^B$. $\kappa^B = 30 k_B T$.

component. It is demonstrated in Fig. 5.5 that when the intrinsic mean curvature of the isotropic membrane component is increased (for fixed reduced volume) the cylindrical membrane protrusions are formed and their length increases with the increase of the intrinsic mean curvature of the anisotropic component.

In the membrane systems, in which the cylindrical membrane tubes are created when the macromolecules (*e.g.* BAR domain proteins) are adsorbed at the membrane surface, the radius of the tubule is determined by the intrinsic curvature of the macromolecule, *i.e.* considering the membrane element containing macromolecule(s) as a nanodomain characterized by proper intrinsic curvature, the tube radius is determined by the intrinsic curvature of nanodomain. In Fig. 5.6 we show that there is a strict relation between the intrinsic curvature of the anisotropic component,D_m^A, and the radius of the tube.

For smaller values of $D_m^A < 5.5$ the cylindrical tube is not observed. For $D_m^A > 9.45$ a tubular protrusion begins to form. The decreasing of the tube radius is coupled to the accumulation of the anisotropic component in small membrane area, indicated by arrows in the lower panel of Fig. 5.6. At $D_m^A = 9.45$ there is a transition transition to the well developed cylindrical tubule. Apart from the values of D_m^A in the vicinity

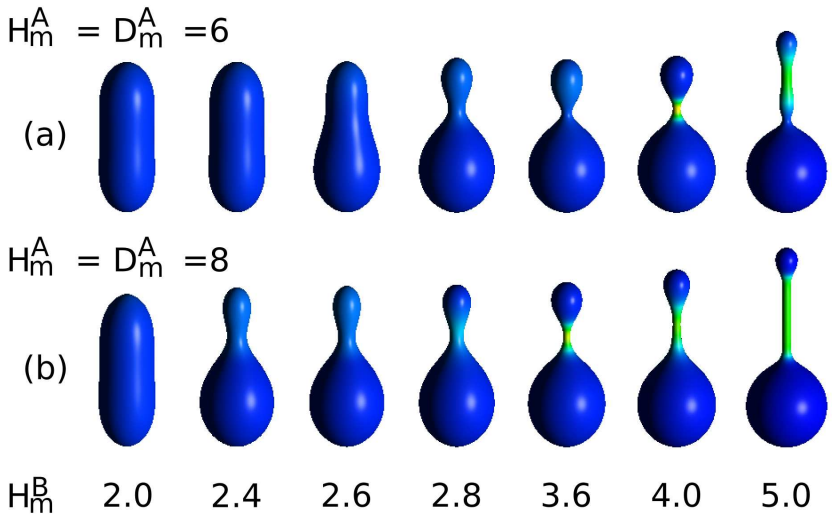

Figure 5.5: The vesicle shapes for different values of the mean curvature of isotropic component H_m^B, and for $v = 0.8$, $\phi = 0.055$, $\kappa^A = 4\kappa^B$ ($\kappa^B = 30k_BT$). The mean curvatures of anisotropic component are: (a) $H_m^A = D_m^A = 6.0$ and (b) $H_m^A = D_m^A = 8.0$.

of the transition value, we can see that for the well developed cylindrical membrane tubes (for $D_m^A > 10$) the radius of the tubular structure decreases linearly with increasing D_m^A. Thus, the results of our theoretical calculations are in qualitative agreement with the experimental predictions showing that the membrane tubular protrusions induced by the membrane bound anisotropic molecules (such as highly anisotropic BAR domain-containing proteins) with larger intrinsic curvature radius (corresponding to smaller D_m^A) generally have larger diameters than do those formed by the molecules characterized by smaller intrinsic curvature radius (i.e. larger D_m^A).

Figs. 5.7 and 5.8 present the shape transformations and redistribution of anisotropic membrane component on the vesicle surface induced by the change of its intrinsic geometry (ellipsoidal nanodomain shape), and change of reduced volume, respectively.

5.1.2 Conclusions

We have shown that accumulation of anisotropic components may lead to formation of thin tubular membrane protrusions. The anisotropy of the membrane components is a necessary condition for creation of the *stable* tubular protrusions in the absence of the external force. When all membrane components are isotropic the stable cylindrical structures may be created only when external force is applied [5, 43, 90–94]. The

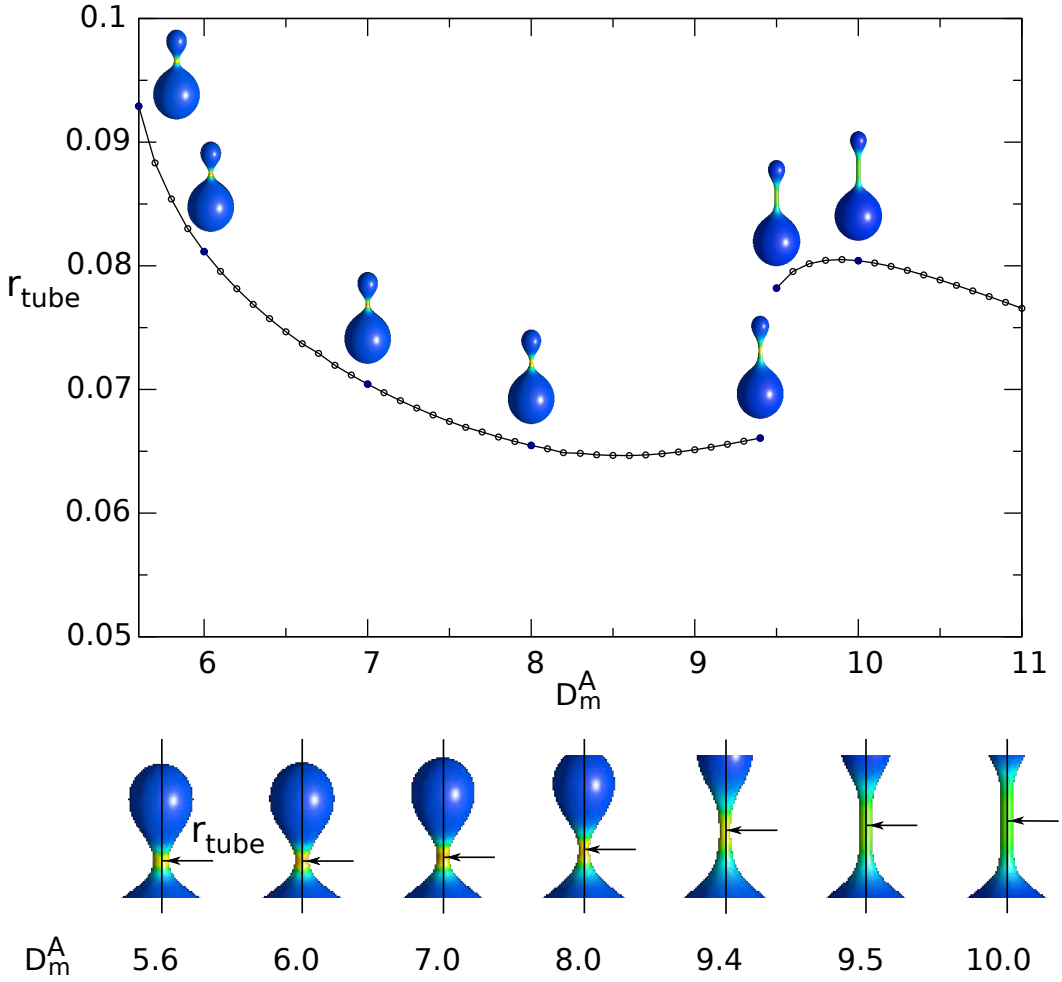

Figure 5.6: The change of the radius of the tubular region of a vesicle as a function of the intrinsic curvature of anisotropic component D_m^a for $v = 0.8$, $\phi = 0.04$, $H_m^B = 4.2$, $D_m^B = 0$, $H_m^A = D_m^A$, $\kappa^A = 4\kappa^B$ ($\kappa^B = 30 k_B T$). The arrows in the lower panel indicates the position on the surface of the vesicle where the radius for the tube was determined.

diameter of the membrane tubular protrusions depends on the intrinsic curvatures of anisotropic components. When the membrane is composed of isotropic components only the *stable* protrusions which are induced without application of external force are composed of a series of connected beads (Fig. 5.9). The tubular protrusions for relatively high reduced volume of the vesicle are not possible in this case.

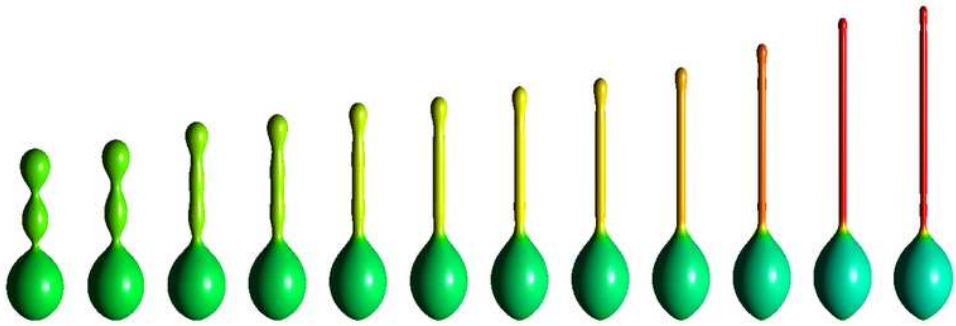

Figure 5.7: The shapes of the vesicles for different values of the curvature deviator. The shapes are calculated for the following values of intrinsic curvature deviator of component A, D_m^A: 0.45, 0.55, 0.65, 0.8, 1.15, 1.30, 1.55, 1.75, 2.00, 2.50, 3.00, 3.45. The calculations were performed for the following parameters $v = 0.64$, $\phi_{tot} = 0.5$, $H_m^A = 8$, $H_m^B = 0$, $D_m^B = 0$, $\kappa = 30 k_B T$.

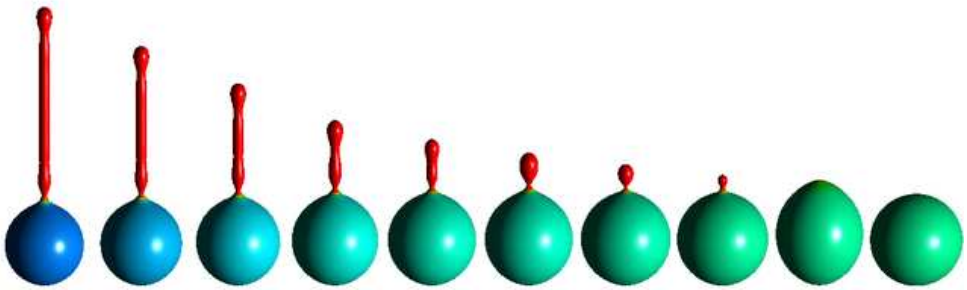

Figure 5.8: The vesicle shapes for calculated for different values of the reduced volume (form left to right) $v = 0.690,\ 0.750,\ 0.810,\ 0.870,\ 0.910,\ 0.920,\ 0.950,\ 0.980,\ 0.990,\ 1.000$. The calculations were performed for $\phi_{max} = 0.35$, $H_m^A = 8$, $H_m^B = 4$, $D_m^A = 0.95$, $D_m^B = 0$, $\kappa = 30 k_B T$.

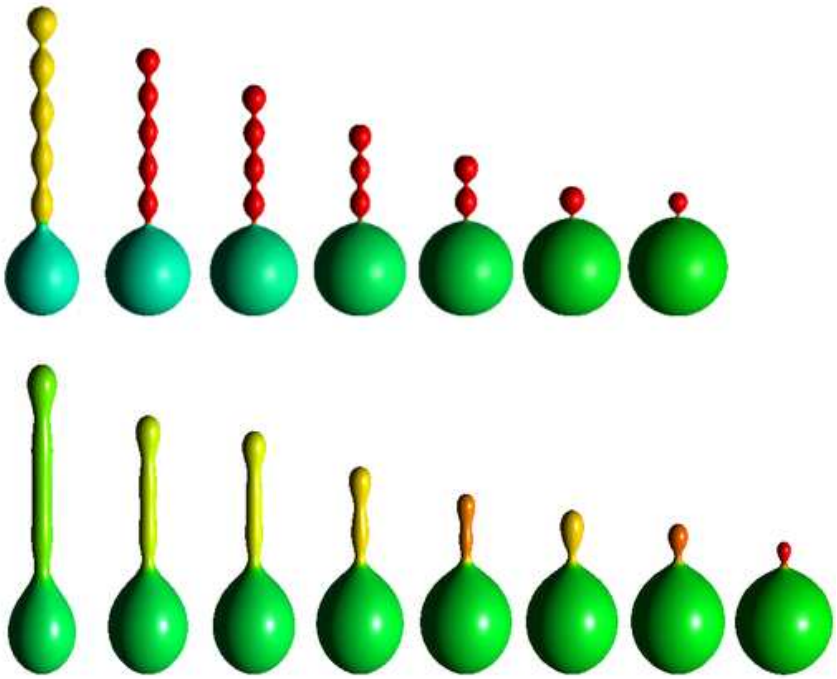

Figure 5.9: Comparison of the calculated membrane protrusion formed in the vesicles with the membrane composed of two isotropic components (upper panel) and mixture of isotropic and anisotropic membrane components (lower panel). The values of reduced volume for the first and the second row are $v = 0.540,\ 0.680,\ 0.725,\ 0.805,\ 0.875,\ 0.920,\ 0.950$ and $v = 0.540,\ 0.680,\ 0.720,\ 0.800,\ 0.870,\ 0.880,\ 0.920,\ 0.960$ respectively. The parameters use in the calculations are $\phi_{max} = 0.5$, $H_m^A = 8$, $H_m^B = 0$, $D_m^A = 0.95$, $D_m^B = 0$.

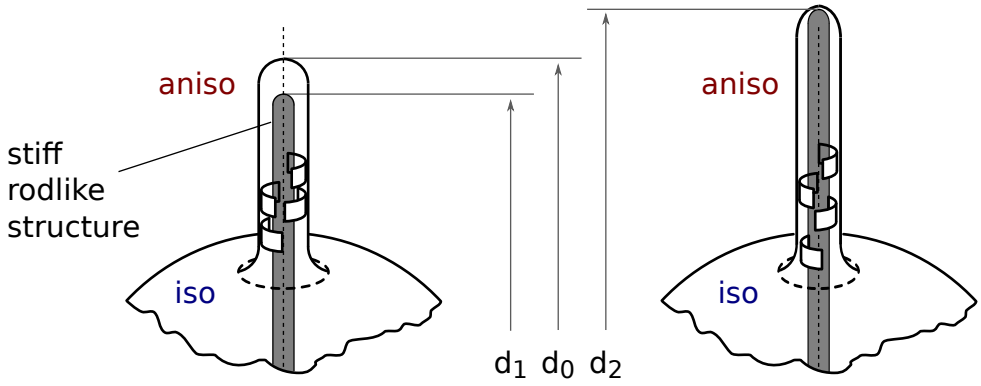

Figure 5.10: Schematic representation of a microtubule growing inside the cylindrical membrane protrusion of the vesicle with two-component membrane. d_1 is the length of the microtubule, d_0 is the length of the membrane protrusion before the application of "pushing" force. d_2 is the length of the membrane protrusion pushing out by microtubule, which is equal to the length of microtubule outside the membrane surface.

5.2 Two-component membrane system with the application of external pulling force

As it was shown in Section 5.1, the accumulation of anisotropic membrane component in two-component membranes composed of at least one anisotropic component, may lead to the formation of the cylindrical protrusions without the application of external pulling/pushing force. In the case of the membranes composed of the two isotropic components cylindrical protrusions can only be obtained with the application of an external puling/pushing force (see Subsection 4.2.4). The intriguing question arises: *what is the influence of the combination of component anisotropy and application of external pulling/pushing force on the component separation process in multicomponent membranes?*[4] This section is devoted to answer this question.

In this section, the behavior of the vesicles with the membrane composed of both isotropic and anisotropic components when external force is applied is investigated. The corresponding system is schematically shown in Fig. 5.10. The results obtained for such systems may shed some light on the phenomena related to the cell and vesicle shape transformations and segregation of membrane components, since biological membranes are usually built of many anisotropic components.

[4]The experimental investiagtions on the Lubrol rafts have shown their accumulation in tubular membrane protrusions (for example, see Ref. [95] and references within).

Lateral segregation of membrane constituents may be induced by coupling between the local curvature of membrane surface and the local concentration of membrane components, characterized by their intrinsic shape, and thus by an intrinsic spontaneous curvature. It is assumed that membrane constituents prefer to occupy the membrane region with a membrane curvature comparable to the intrinsic curvature of the component [35]. The physical aspects of formation of membrane tubular structures are presented in the review [96].

We have studied three different mechanisms of lateral redistribution and segregation of the membrane components induced by:

(i) the elongation of the vesicle, which corresponds to the growth of the microtubule inside the vesicle,

(ii) the change of the reduced volume of the vesicle with fixed length, which corresponds to the case, when the microtubule inside the vesicle has fixed pole to pole distance and the volume of the vesicle is changed,

(iii) the change of the intrinsic shape of membrane constituents of the vesicle with pole to pole distance.

5.3 Results

(i) Two-component vesicle with membrane components characterized by large intrinsic curvature of *anisotropic* membrane component of cylindrical shape,($H_m^A = D_m^A$), large bending rigidity, κ^A, and small intrinsic curvature of *isotropic* membrane component of spherical geometry, ($H_m^B \neq 0$, $D_m^B = 0$) and small bending rigidity κ^B is ***elongated*** in the direction of its axis of symmetry.

Here we present the results where ***the entropy of mixing is not taken into account.*** The fixed parameters are: reduced volume $v = 0.6$, concentration of anisotropic component $\phi_{tot} = 0.15$, mean intrinsic curvature of isotropic component $H_m^B = 1$, mean intrinsic curvature of anisotropic component $H_m^B = 8$, deviatoric intrinsic curvature of isotropic component $D_m^B = 0$, deviatoric intrinsic curvature of anisotropic component $D_m^A = 8$, bending rigidity of isotropic component $\kappa^B = 30 k_B T$, and bending rigidity of anisotropic component $\kappa^A = 8\kappa^B$. The reduced distance between the poles of the vesicle (d) changes within the range of $6.2 < d < 8.6$. Initially the vertical length of the vesicle with tubular protrusion which is induced by anisotropic membrane component ($h = 6.25$) is longer than the length of the microtubule inside the vesicle ($d = 5.1$), see

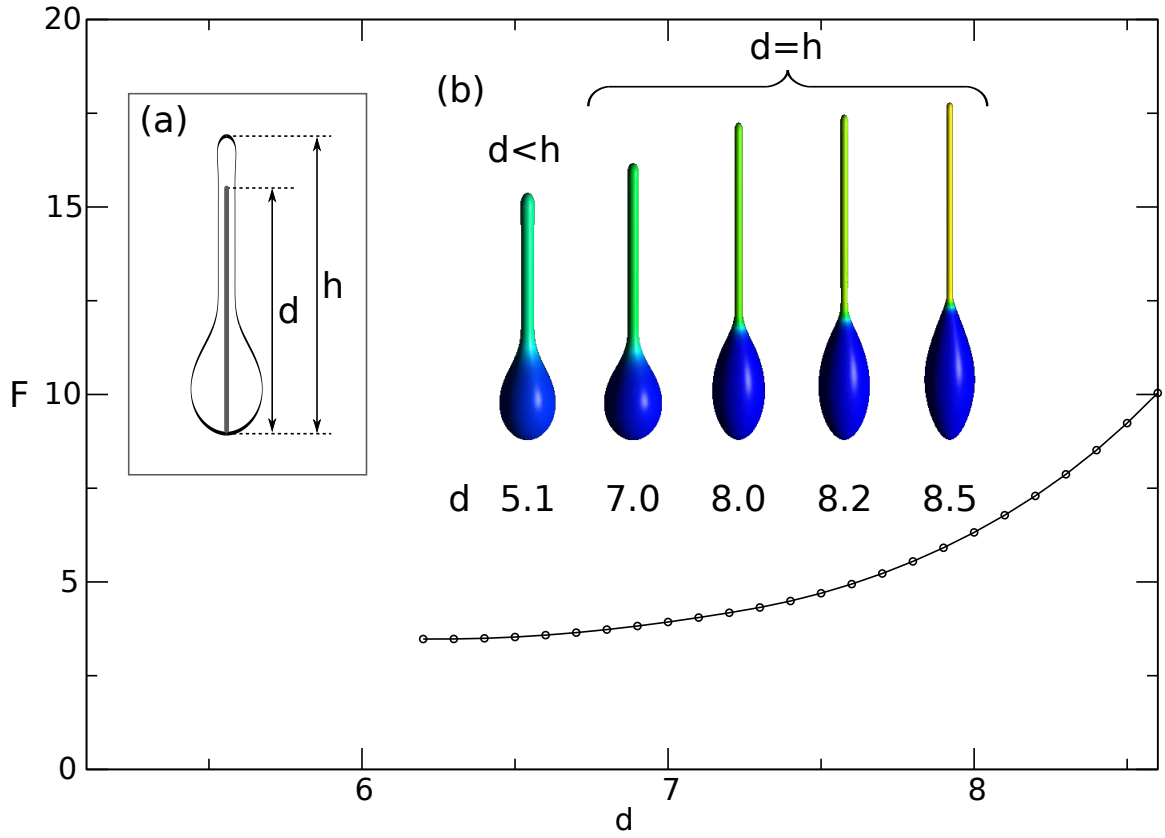

Figure 5.11: The dependence of the membrane energy as a function of the length of microtubule inside the vesicle. (a) A schematic view of the vesicle with tubular protrusion and growing microtubule inside. (b) Change of the vesicle shape and the concentration of the anisotropic component within the tube induced by the growth of microtubule. The calculation were performed for the following parameters $v = 0.6$, $\phi_{tot} = 0.15$, $H_m^B = 1$, $D_m^B = 0$, $H_m^A = 8$, $D_m^A = 8$, $\kappa^A = 8\kappa^B$ and $\kappa^B = 30 k_B T$.

Fig. 5.11. The entropy of mixing of membrane components is not considered as already mentioned above.

(ii) Fig. 5.12, similarly to Fig. 5.11, shows the vesicle shape transformation and the corresponding lateral redistribution and segregation of membrane components. Fig. 5.12 represents the different mechanism of segregation caused by the change of the ***reduced volume*** of the vesicle including microtubule inside. Again, initially the vertical length of the vesicle(together with the tubular protrusion) is longer then the length of the microtubule (d), $h = 6.25$. The entropy of mixing is not taken into account. By increasing the reduced volume, the radius of tube is changed in such a way (decreases) that the membrane component with high intrinsic curvature (anisotropic component) is accumulated in the protrusion. As the consequence, the radius of the

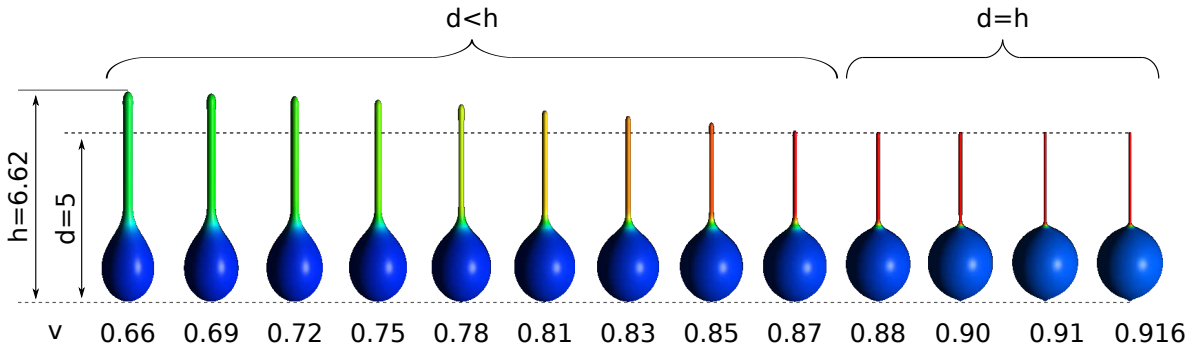

Figure 5.12: The shapes of vesicles calculated for different values of the reduced volume v. The microtubule of the length $d = 5$ is present inside the vesicle. The calculation were performed for the following parameters $\phi_{tot} = 0.15$, $H_m^B = 1$, $D_m^B = 0$, $H_m^A = 8$, $D_m^A = 8$, $\kappa^A = 8\kappa^B$ and $\kappa^B = 30 k_B T$.

tubular protrusion is decreased. Figs. 5.12 and 5.13 show the change of the tube radius and the concentration as a function of increasing reduced volume.

The change of the vesicle shape with the microtubule inside the vesicle induced by the change of the reduced volume is depicted also in Fig. 5.14. We have also performed similar calculations with the entropy of mixing taken into account. The change of the slope on the curves for both the local concentration of anisotropic membrane component and the tube radius at $v = 0.75$ (lower panel in Fig. 5.14), is due to the fact, that at this point the length of the vesicle becomes equal to the length of microtubule

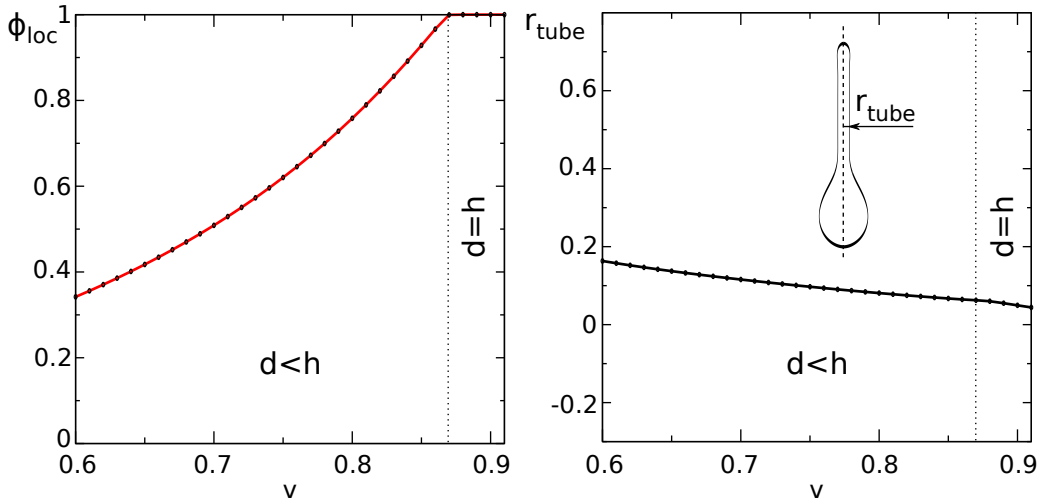

Figure 5.13: Change of the tube radius and concentration of anisotropic membrane component in the tube as a function of reduced volume. The calculation were performed for the same parameters as previously on Fig. 5.12.

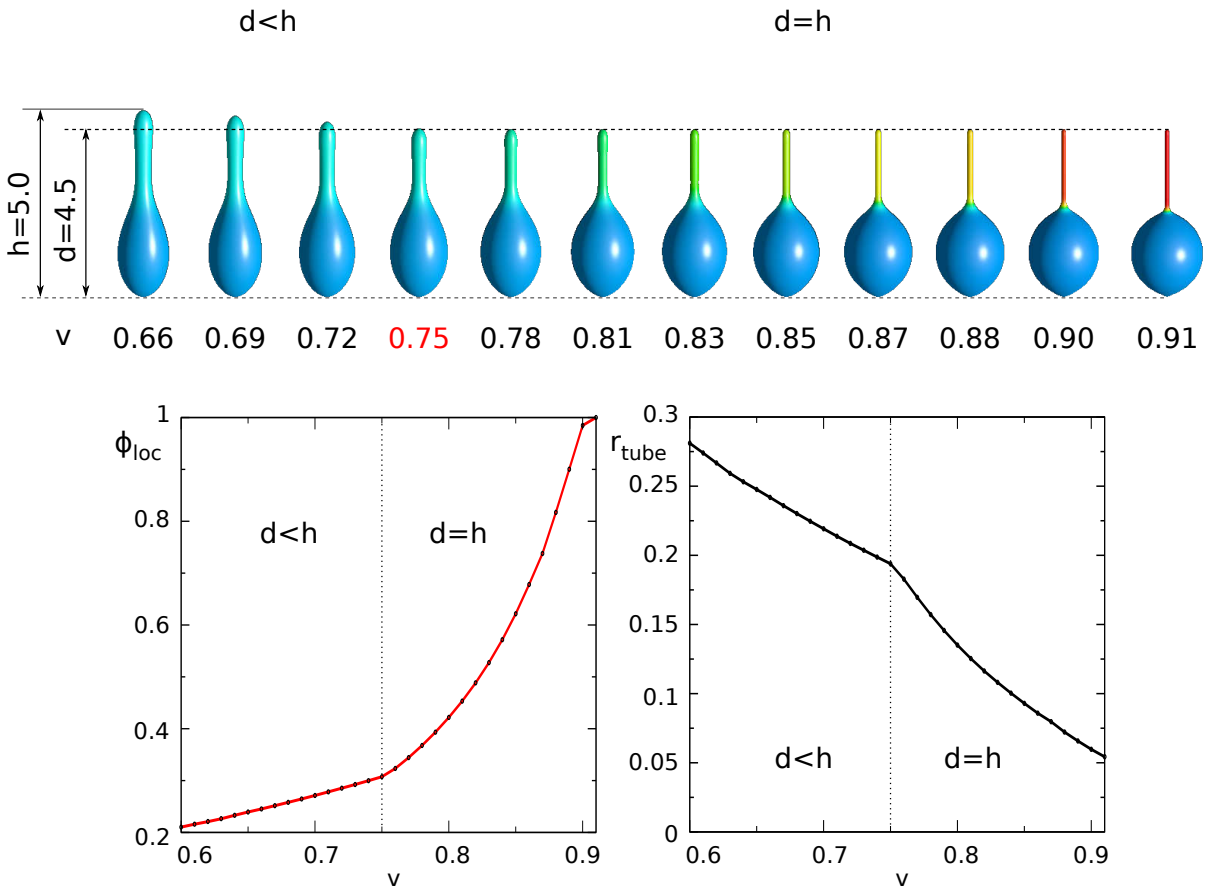

Figure 5.14: The shapes of the vesicles calculated for different values of the reduced volume v, when the microtubule of the length $d = 4.5$ is present inside the vesicle. The entropy of mixing is taken into account. Lower panel shows the change of the tube radius and concentration of anisotropic component in the tube region with the change of reduced volume. The calculation were performed for the following parameters $\phi_{tot} = 0.15$, $H_m^B = 1$, $D_m^B = 0$, $H_m^A = 8$, $D_m^A = 8$, $\kappa^A = 8\kappa^B$, $\kappa^B = 30 k_B T$.

($h = d$) inside the vesicle. For $v > 0.75$ the pole to pole distance remains fixed and equal to the length of a microtubule. The increase of the reduced volume induces the change in the local membrane curvature (the curvature of membrane protrusion increases). This causes the accumulation of membrane component with higher intrinsic curvature in this region.

In Fig. 5.15 we compare the dependence of the local curvature of the tubular protrusion for different values of the reduced volume in two cases where the entropy of mixing present and absent in the calculations. Red points denote the tube curvature which is nearly equal to the curvature of anisotropic membrane component. The reduced volume is $v = 0.82$ which corresponds to the value of the local concentration

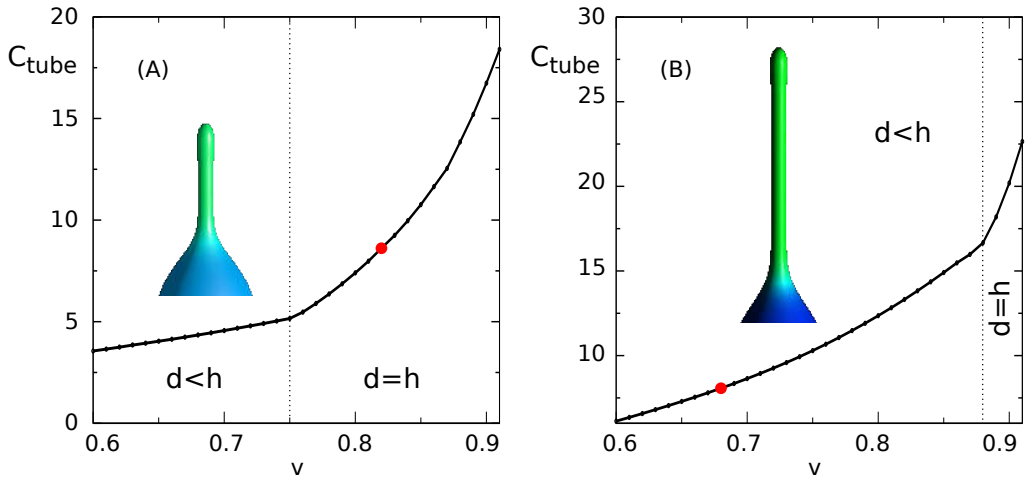

Figure 5.15: The curvature of the vesicle tubular protrusion as a function of reduced volume v. (A) corresponds to the case when entropy of mixing is present. (B) panel shows curvature plot without the taking into account the entropy of mixing. Red points denote the tube curvature nearly equal to the curvature of anisotropic component and the corresponding values of reduced volume for each case. The calculation were performed for the following model parameters $\phi_{tot} = 0.15$, $H_m^B = 1$, $D_m^B = 0$, $H_m^A = 8$, $D_m^A = 8$, $\kappa^A = 8\kappa^B$.

$\phi_{loc} = 0.45$ ($h = d \approx 4.5$). For the case, where the entropy of mixing is not taken into account, $v = 0.68$ which corresponds to $\phi_{loc} = 0.47$ ($h = 6.13$, $d = 5.0$). The anisotropic membrane component is fully accumulated in the region of tubular protrusion, however even if the local curvature of the tubular protrusion is close to the intrinsic curvature of membrane constituents, there is still a significant amount of isotropic component present in it. The reason might be a relatively large difference in curvatures and the shape of membrane components ($H_m^B = 1, D_m^B = 0$ (nearly flat) vs. $H_m^A = 8, D_m^A = 8$ (cylindrical with high curvature)).

It will be interesting to examine: *what will be the influence of mictorubule growth on the component segregation?* We chose the vesicle with small value of the deviatoric curvature $D_m^A = 1.5$ and large reduced volume $v = 0.94$ (see first configuration from the left-hand side in Fig. 5.17). Fig. 5.16 shows the shape transformation and the segregation of membrane components caused by the microtubule growing inside the vesicle. The elongation of the vesicles induces the segregation of the membrane component. Note that the anisotropic component is accumulated at the tip of the cylindrical protrusion.

(iii) The segregation of components in two-component membrane system might be

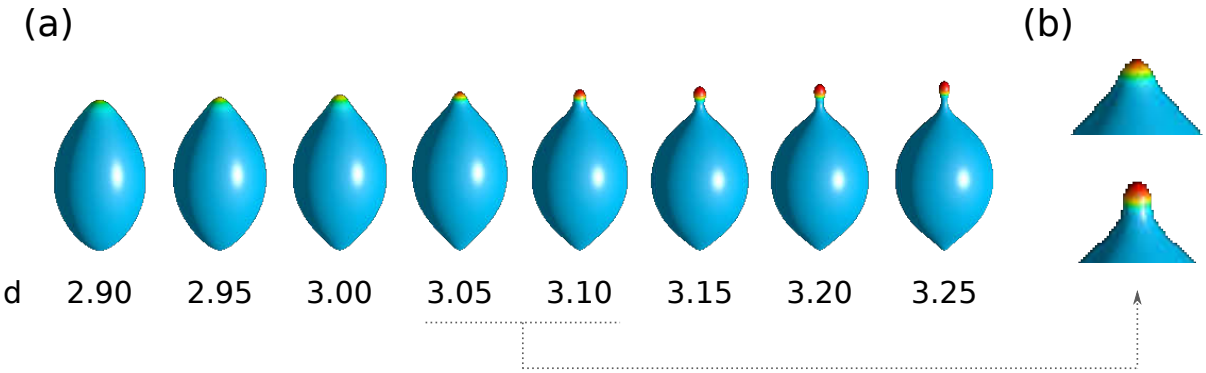

Figure 5.16: (a) Shapes of the vesicles calculated for different length of the microtubule d. (b) Zoomed region of membrane, where the accumulation of anisotropic membrane component appears. The model parameters used in the calculations are $v = 0.94$, $\phi_{tot} = 0.15$, $H_m^B = 1$, $H_m^A = 8$, $D_m^B = 0$, $D_m^A = 1.5$, $\kappa^A = 8\kappa^B$ and $\kappa^B = 30k_BT$.

the result of the change of intrinsic shape of one or both membrane components. Fig. 5.17a shows the shape transformation and the segregation of membrane components induced by the change of ***intrinsic shape*** of anisotropic membrane component, D_m^A. Microtubule inside the vesicle with a relatively large reduced volume $v = 0.93$ has a fixed length, which is equal to the pole to pole distance ($h = d$), and thus does not influence the membrane component segregation. In this case the formation of the membrane tubular protrusion is induced only by anisotropic properties of a component. The geometry changes from ellipsoidal ($H_m^A \neq D_m^A \neq 0$) to cylindrical ($H_m^A = D_m^A$). As in previous case, the anisotropic membrane component accumulates in the tip of the tube, and for small value of the deviatoric curvature ($D_m^A = 1.5$) its

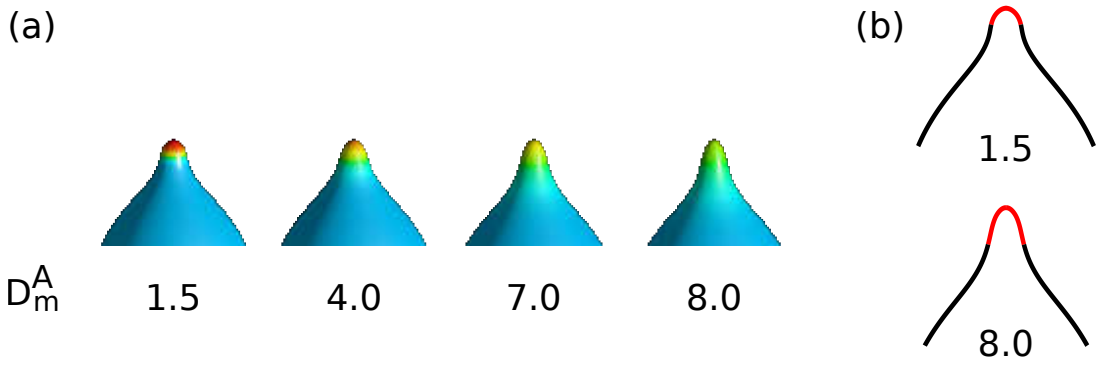

Figure 5.17: Shapes of the vesicles calculated for different values of deviatoric curvature D_m^A (a). Panel (b) shows the limiting shapes of vesicle profiles for $D_m^A = 1.5$ and 8.0, respectively. The parameters used in the calculations are $v = 0.93$, $\phi_{tot} = 0.15$, $H_m^B = 1$, $H_m^A = 8$, $D_m^B = 0$, $d = 3.15$, $\kappa^A = 8\kappa^B$ and $\kappa^B = 30k_BT$.

local concentration in the tip of the tubular protrusion (creating locally curved region of membrane, with the curvature comparable to the intrinsic curvature of anisotropic component, see Fig. 5.17b) reaches $\phi_{loc} \approx 100\%$.The anisotropic membrane component (with the increasing of its deviatoric intrinsic curvature) starts changing locally the membrane curvature inducing the formation of membrane region suitable for the growth of membrane tubular protrusion. For $D_m^A = 8.0$ the local concentration of anisotropic component on the tip of the vesicle is $\phi_{loc} = 0.64$.

5.3.1 Conclusions

Segregation of the membrane components in two-component membrane vesicles, where one of the components is anisotropic with large intrinsic curvature might be induced by the growth of the microtubule inside the vesicle. Growth of the microtubule regulates the radius of the membrane tubular protrusion, and thus, influences the migration of the anisotropic membrane components to the region of membrane, where the local curvature is large.

CHAPTER 6

Summary and conclusions

We have theoretically investigated the lateral redistribution and segregation of membrane components in vesicles with two-component model membrane. The distribution of the membrane components was shown to be coupled to the shape transformation of the vesicles. Our studies based on two theoretical models: the *spontaneous curvature model* and the *dieviatoric elasticity model*. We mainly focused on the explanation of experimentally observed phenomena occurring in biological and model multicomponent membrane systems.

The main results presented in this Thesis can be **summarized** as follows:

- studies of component segregation of two-component membrane vesicles within the framework of *spontaneous curvature model* indicate that in the case of *absence of external pulling/pushing force*, with the change of membrane shape the membrane components start to migrate to regions with local curvature that matches better their intrinsic (spontaneous) curvature, and simultaneously with the migration (and hence the change of the local concentration) the local membrane curvature is changed. Therefore, the vesicles with membrane components, whose spontaneous (intrinsic) curvature significantly differs from each other, are susceptible for separation of components when the shape of the vesicle might be considered as one composed of parts with different local curvatures.
  In the case of the *presence of external pulling/pushing force*, for similar assumptions regarding the spontaneous (intrinsic) curvature of the membrane components, the elongation of a vesicle may lead to formation of tubular protrusions occupied mainly by the component with larger spontaneous curvature (Fig. 6.1b).

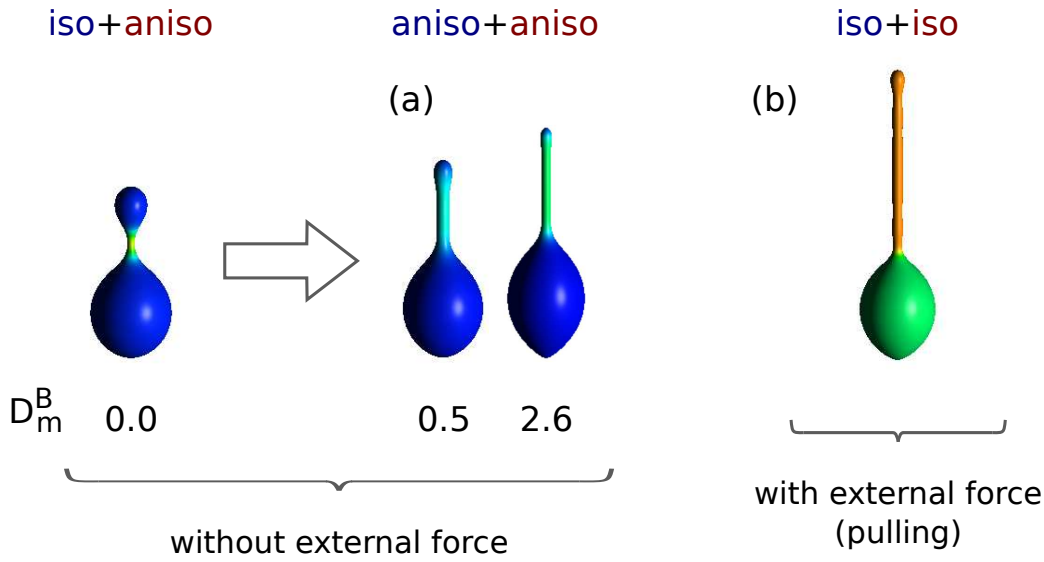

Figure 6.1: Similarities in vesicle shapes obtained without (a) and with (b) application of external force. For change of intrinsic geometry of component from spherical (isotropic) to ellipsoidal (anisotropic) corresponds the change of component deviator from $D_m^B = 0.0$ to $D_m^B \neq 0.0$ ($D_m^B = 0.5, 2.6$).

- the investigation of segregation of components in two-component vesicles within the framework of *deviatoric elasticity model* indicate that, again, in the case of *absence of external pulling/pushing force*, the accumulation of anisotropic components may lead to the formation of thin stable tubular membrane protrusions (Fig. 6.1a). When membrane vesicle consist of only anisotropic components, the vesicle shape becomes similar to the shape obtained by the elongation of vesicle made of both isotropic component.

  In the case when *presence of external pulling/pushing force* is applied the tubular protrusions occupied by the component with larger intrinsic deviatoric curvature are formed.

We also derived the *general expression* for function of the local relative concentration for two-component model membrane (Appendix D).

The most important general **conclusions** are as follows:

- The separation of membrane component in multicomponent membranes depends on the ratio between the vesicle size and the area of the membrane components (nanodomains), and the intrinsic shapes of membrane components.

- The shape transformation of multicomponent biological membranes may induce the lateral redistribution and segregation of the membrane components. However, the change of the local concentration of membrane components influences the local curvature of the membrane region as well.

To conclude, this thesis contributes to the current knowledge about the lateral redistribution and segregation of the membrane components in cells and multicomponent model lipid membranes. Understanding the mechanism of lateral segregation of membrane components may have aa important impact in development of material sciences. Lipid vesicles seem to be promising candidates for specialized functional biocompatible materials, which may be tuned and used, for example, for target drug delivery (cancer treatment) [97], biosensing applications [98] or preparation of artificial cells.

Author's publications

Results presented in the thesis have been published in the following papers:

1. *N. Bobrovska*, W. Góźdź, V. Kralj-Iglič and A. Iglič, "On the role of anisotropy of membrane components in formation and stabilization of tubular structures in multicomponent membranes", *PLoS ONE*, 2013, *8(9)*, e73941

2. D. Kabaso, *N. Bobrovska*, W. Góźdź, E. Gongadze, V.Kralj-Iglič , R. Zorec, A. Iglič, "The transport along membrane nanotubes driven by the spontaneous curvature of membrane components", Bioelectrochemistry, 2012, *87*, 204-210

3. D. Kabaso, *N. Bobrovska*, W. Góźdź, N. Gov, V. Kralj-Igliv̌, P. Veranič, A. Iglič, "On the role of membrane anisotropy and BAR proteins in the stability of tubular membrane structures", Journal of Biomechanics, 2012, *45*, 231-238

4. W. T. Góźdź, *N. Bobrovska*, A. Ciach, "Separation of components in lipid membranes induced by shape transformation", Journal of Chemical Physics, 2012, *137*, 015101

APPENDIX **A**

Basics of differential geometry of surfaces

A.1 Surface and principal curvatures

A two-dimensional surface embedded in three-dimensional Euclidean space is mathematically defined by

$$\mathbf{r} = (x(u,v), y(u,v), z(u,v)) \tag{A.1}$$

where u and v are coordinates on the surface. For any point of the surface one can define two tangent vectors

$$\mathbf{r}_u = \frac{\partial \mathbf{r}}{\partial u} = \left(\frac{\partial x}{\partial u}, \frac{\partial y}{\partial u}, \frac{\partial z}{\partial u}\right), \tag{A.2}$$

$$\mathbf{r}_v = \frac{\partial \mathbf{r}}{\partial v} = \left(\frac{\partial x}{\partial v}, \frac{\partial y}{\partial v}, \frac{\partial z}{\partial v}\right), \tag{A.3}$$

which, in general, are not unit nor orthogonal vectors. They defined a tangent plane in this point of a surface.

The normal vector, which is perpendicular to tangent plane is

$$\mathbf{n} = \frac{\mathbf{r}_u \times \mathbf{r}_v}{|\mathbf{r}_u \times \mathbf{r}_v|}. \tag{A.4}$$

The normal plane is the plane, which contains normal vector $\mathbf{n}$. The intersection of the normal plane and the surface define a curve with curvature $1/R$, where R is the radius of curvature of this curve in the point P. The expression for curvature is

$$\frac{1}{R} = \frac{Ldu^2 + 2Mdudv + Ndv^2}{Edu^2 + 2Fdudv + Gdv^2}, \tag{A.5}$$

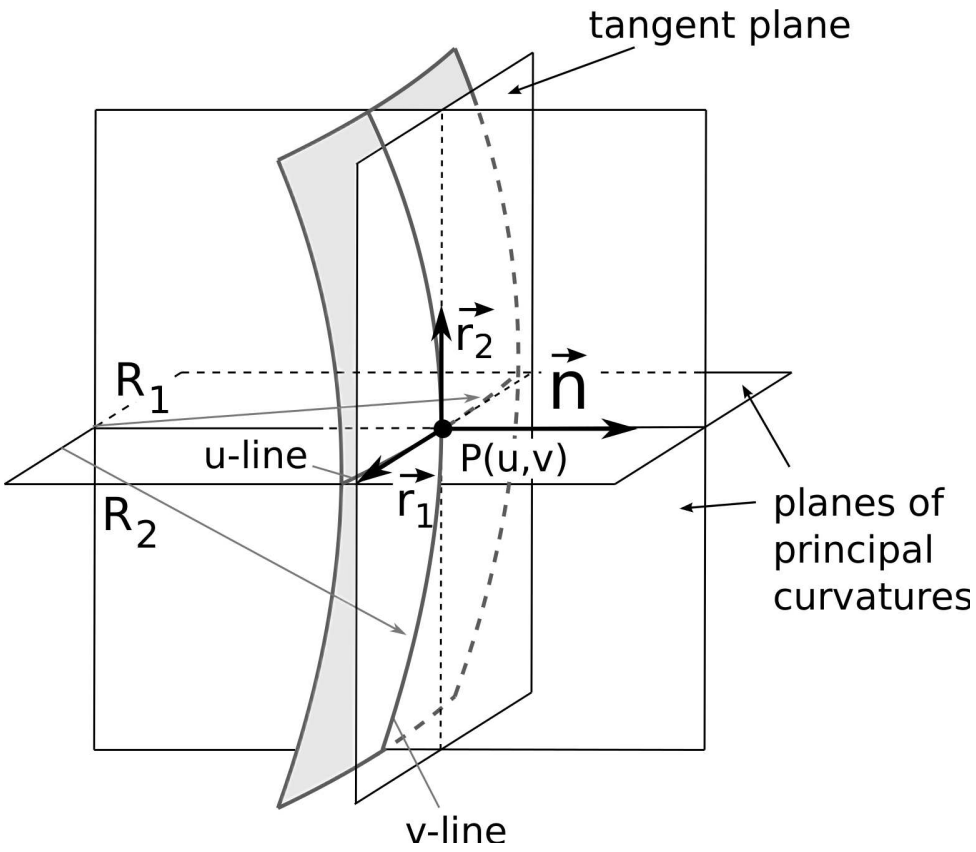

Figure A.1: Surface, characterized by principal radii R_1 and R_2, and its element, characterized by intrinsic principal radii R_{1m} and R_{2m}.

where $E = \mathbf{r}_u \cdot \mathbf{r}_u$, $F = \mathbf{r}_u \cdot \mathbf{r}_v$, $G = \mathbf{r}_v \cdot \mathbf{r}_v$, $L = \mathbf{n} \cdot \mathbf{r}_{uu}$, $E = \mathbf{n} \cdot \mathbf{r}_{uv}$ and $E = \mathbf{n} \cdot \mathbf{r}_{vv}$.

Principal curvatures of the surface, $C_1 = 1/R_1$ and $C_2 = 1/R_2$, are defined by two orthogonal normal planes, see Fig. A.1.

These curvatures are the extrema of all possible curvatures. The mean value of C_1 and C_2

$$H = \frac{1}{2}(C_1 + C_2) \tag{A.6}$$

is called the mean curvature, while their product

$$K = C_1 C_2 \tag{A.7}$$

is called the Gaussian curvature.

A.2 Gauss-Bonnet theorem

In general, the Gauss-Bonnet theorem states that sum of the integrals of the Gaussian curvature,K, of a compact Riemannian manifold M, and geodesic curvature, k_g, along

its boundary,∂M, and sum of the jump angles of this boundary,α_i , is proportional to the Euler characteristic,$\chi(M)$, of the manifold.

$$\int_M K dA + \int_{\partial M} k_g ds + \sum_i \alpha_i = 2\pi\chi(M). \tag{A.8}$$

When the manifold M is a closed regular surface, the expression above becomes

$$\int_M K dA = 2\pi\chi(M). \tag{A.9}$$

The Euler characteristic χ is a topological invariant, it only changes with the change of the topology of the surface. For continuous deformations it remains constant. For a regular surface, it takes form

$$\chi = 2(N - g), \tag{A.10}$$

where N is the number of objects, and g is the genus of the surface, *i.e.* the number of handles or holes. For instance, the Euler characteristic for the sphere is $\chi(\text{sphere}) = 2$, a one-handle torus $\chi(\text{1-torus}) = 0$ and a two-handle torus $\chi(\text{2-torus}) = -2$ (see Fig. A.2).

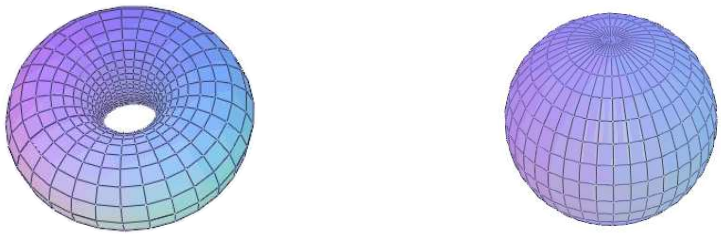

Figure A.2: Euler characteristics for a torus and a sphere.

APPENDIX **B**

Derivations for Eq. (2.7)

The mismatch tensor, its trace, squared trace and determinant are give as follows:

$$\underline{M} = \begin{bmatrix} C_{1\mathrm{m}}\cos^2\omega + C_{2\mathrm{m}}\sin^2\omega - C_1 & C_{1\mathrm{m}}\sin\omega\cos\omega - C_{2\mathrm{m}}\sin\omega\cos\omega \\ C_{1\mathrm{m}}\sin\omega\cos\omega - C_{2\mathrm{m}}\sin\omega\cos\omega & C_{1\mathrm{m}}\sin^2\omega + C_{2\mathrm{m}}\cos^2\omega - C_2 \end{bmatrix},$$

$$\mathrm{Tr}\underline{M} = C_{1\mathrm{m}} + C_{2\mathrm{m}} - C_1 - C_2, \tag{B.1}$$

$$(\mathrm{Tr}\underline{M})^2 = 4(H - H_m)^2, \tag{B.2}$$

$$\mathrm{Det}\underline{M} = (H^2 - 2HH_m + H_m^2) - D^2 + 2DD_m\cos 2\omega - D_m^2. \tag{B.3}$$

Finally, we get the expression for the elastic energy per membrane element (Eq. (2.7)):

$$\begin{aligned} w \quad &= \mu_0 + \frac{K_1}{2}(\mathrm{Tr}\underline{M})^2 + K_2\,\mathrm{Det}\underline{M} = \\ &= \mu_0 + \frac{K_1}{2}4(H - H_m)^2 + K_2\left\{(H - H_m)^2 - D^2 + 2DD_m\cos 2\omega - D_m^2\right\} = \\ &= \mu_0 + (2K_1 + K_2)(H - H_m)^2 - K_2(D^2 - 2DD_m\cos 2\omega + D_m^2). \end{aligned} \tag{B.4}$$

APPENDIX C

Limiting case for DE model

C.1 General energy equation for nanodomain

$$E_i = da_0 \left[(2K_1 + K_2)(H - H_m)^2 - K_2(D^2 - 2DD_m \cos 2\omega + D_m^2) \right], \tag{C.1}$$

where ω is the angle of rotation of nanodomain, da_0 is area of small plate like nanidomain.

For fully oriented nanodomain $\cos 2\omega = 1$ ($\omega = 0$ or $\omega = \pi$) and Eq. (2.7) becomes

$$E_i = da_0 \left[(2K_1 + K_2)(H - H_m)^2 - K_2(D - D_m)^2 \right]. \tag{C.2}$$

If $K_1 = -K_2 = K$, than

$$E_i = da_0 K \left[(H - H_m)^2 + (D - D_m)^2 \right]. \tag{C.3}$$

C.2 Limit for Helfrich energy

The Eq. (C.1) represent a general form for membrane free energy, which takes into account anisotropy of components. If we assume that membrane components are istropic only, then their intrinsic principal curvatures are equal $C_{1m} = C_{2m} = C_m$, thus $D_m = 0$ and $H_m = C_m$.

C.2.1 Partial case

Let us consider only part of Eq. (C.3) $K[(H-H_m)^2+(D-D_m)^2]$, with this assumption and $D^2 = H^2 - C_1C_2$ it becomes

$$\begin{aligned} w' &= K\left[(H-H_m)^2 + D^2\right] = \\ &= K\left[H^2 - 2HH_m + H_m^2 + H^2 - C_1C_2\right] = \\ &= K\left[2H^2 - 2HH_m + H_m^2 - C_1C_2\right] = \\ &= K\left[\frac{1}{2}\left(4H^2 - 4HH_m + H_m^2\right) + \frac{H_m^2}{2} - C_1C_2\right] = \\ &= K\left[\frac{1}{2}(2H - H_m)^2 + \frac{H_m^2}{2} - C_1C_2\right]. \end{aligned} \tag{C.4}$$

Finally we get the equation similar to the Helfrich free energy [99]:

$$w' = K\int\left[\frac{1}{2}(2H-H_m)^2 - C_1C_2\right] + K\frac{H_m^2}{2}dA. \tag{C.5}$$

Term with H_m^2 is constant for the constant area, therefore we omit it. If we assume that $k_c = K$ and $k_g = -K$,

$$w' = \frac{k_c}{2}\int(2H-H_m)^2dA + k_g\int C_1C_2dA = \tag{C.6}$$

$$= \frac{k_c}{2}\int(2H-C_m)^2dA + k_g\int C_1C_2dA \tag{C.7}$$

it means that $k_c = -k_g$.

C.2.2 General case

In general we start from [66]:

$$\begin{aligned} &(2K_1+K_2)(H-H_m)^2 - K_2D^2 = \\ &= (2K_1+K_2)(H^2 - 2HH_m + H_m^2) - K_2H^2 + K_2C_1C_2 = \\ &= 2K_1(H^2 - 2HH_m + H_m^2) + K_2(H^2 - 2HH_m + H_m^2) - K_2H^2 + K_2C_1C_2 = \\ &= K_1(2H^2 - 4HH_m + 2H_m^2) + \frac{K_2}{2}(2H^2 - 4HH_m + 2H_m^2) - K_2H^2 + K_2C_1C_2 = \\ &= K_1(4H^2 - 4HH_m + H_m^2) - K_1 2H^2 + K_1H_m^2 + \\ &+\frac{K_2}{2}(4H^2 - 4HH_m + H_m^2) - \frac{K_2}{2}2H^2 + \frac{K_2}{2}H_m^2 - K_2H^2 + K_2C_1C_2 = \\ &= \left(K_1 + \frac{K_2}{2}\right)(2H-H_m)^2 - 2(K_1+K_2)H^2 + \left(K_1+\frac{K_2}{2}\right)H_m^2 + K_2C_1C_2 = \\ &= \left[\left(\frac{2K_1+K_2}{2}\right)(2H-H_m)^2 + H_m^2\right] + K_2C_1C_2 - 2(K_1+K_2)H^2. \end{aligned} \tag{C.8}$$

Let us write Eq. (C.8) in Helfrich form [42]:

$$\left(\frac{2K_1+K_2}{2}\right)(2H-H_m)^2+\left(\frac{2K_1+K_2}{2}\right)H_m^2+K_2C_1C_2-2(K_1+K_2)H^2=$$
$$=\left[\left(\frac{2K_1+K_2}{2}\right)-\left(\frac{K_1+K_2}{2}\right)4H^2\right]-\left(\frac{2K_1+K_2}{2}\right)4HH_m+(2K_1+K_2)H_m^2+K_2C_1C_2=$$
$$=\underbrace{\left\{\left[\frac{K_1}{2}4H^2-\left(\frac{2K_1+K_2}{2}\right)4HH_m+\cdots\right]+K_2C_1C_2\right\}}_{Helfrich\ form}+(2K_1+K_2)H_m^2. \tag{C.9}$$

To find H_m we have to answer the following question. What should be H_m in the second term to give $(K_1/2)4HC_0$?

$$\left(\frac{2K_1+K_2}{2}\right)H_m=\frac{K_1}{2}C_0$$
$$H_m=\frac{K_1C_0}{2K_1+K_2}.$$

Add and subtract $(K_1/2)C_0^2$ into Eq. (C.9).

$$\left\{\frac{K_1}{2}\left(4H^2-4HC_0+C_0^2\right)+K_2C_1C_2\right\}+ \tag{C.10}$$
$$+(2K_1+K_2)\left(\frac{K_1}{2K_1+K_2}+C_0\right)^2-\frac{K_1}{2}C_0^2= \tag{C.11}$$
$$=\left\{\frac{K_1}{2}(H-C_0)^2+K_2C_1C_2\right\}-\frac{(K_1^2-K_2)}{2K_1+K_2}C_0^2. \tag{C.12}$$

The constant term $[(K_1^2-K_2)/(2K_1+K_2)]C_0^2$ does not depend on H and can be omitted. Finally,

$$C_0=\frac{(2K_1+K_2)}{K_1}H_m. \tag{C.13}$$

APPENDIX **D**

General expression for function of the local relative concentration of component A for two-component model membrane

The energy of membrane is taken in form Eq. (C.3)

$$E_{mem} = K \int \left[(H - H_m)^2 + (D - D_m)^2 \right] dA. \tag{D.1}$$

We assume that H_m and D_m are linearly dependent from the concentration function ϕ:

$$H_m(\phi) = (H_m^A - H_m^B)\phi + H_m^B, \tag{D.2}$$

$$D_m(\phi) = (D_m^A - D_m^B)\phi + D_m^B. \tag{D.3}$$

The energy of entropy of mixing is

$$E_{entr} = n_s kT \int \left[\phi \ln \phi + (1 - \phi) \ln(1 - \phi) \right] dA, \tag{D.4}$$

where n_s is constant parameter with dimension of $1/(R)^2$. The limitation is $0 < \phi < 1$. The total energy of membrane is $E_{tot} = E_{mem} + E_{entr}$. Eq. (D.1) can be written as follows:

$$E_{mem} = K \int \left[(H^2 + 2HH_m + H_m^2) + (D^2 + 2DD_m + D_m^2) \right] dA = \tag{D.5}$$

$$= K \int \left[H^2 + D^2 + \beta(\beta - 2H) + \bar{\beta}(\beta \bar{} 2D) + \right. \tag{D.6}$$

$$\left. + 2\phi(\alpha(\beta - H) + \bar{\alpha}(\beta \bar{} D)) + \phi^2(\alpha^2 + \bar{\alpha}^2) \right] dA, \tag{D.7}$$

where $H_m^A - H_m^B = \alpha$, $H_m^B = \beta$, $D_m^A - D_m^B = \bar{\alpha}$ and $D_m^B = \bar{\beta}$.
Euler equation gives $\partial E_{tot}/\partial\phi = 0$. The additional condition is $\int \phi dA = \phi_{tot}$.

$$\frac{\partial E_{tot}}{\partial \phi} = 2K[(\alpha(\beta - H) + \bar{\alpha}(\bar{\beta} - D)) + \phi(\alpha^2 + \bar{\alpha}^2)] - n_s kT \ln \frac{\phi}{1-\phi} + \lambda = 0. \tag{D.8}$$

For the sake of simplicity denote $\eta = (2K/n_s kT)[\alpha(\beta - H) + \bar{\alpha}(\bar{\beta} - D) + (\lambda/2K)]$, $\xi = (-2K/n_s kT)(\alpha^2 + \bar{\alpha}^2)$.
We get

$$-\eta + \xi\phi + \ln \frac{\phi}{1-\phi} = 0. \tag{D.9}$$

We can rewrite the Eq. (D.9) as

$$\ln \frac{\phi}{1-\phi} + \eta\xi = \eta \tag{D.10}$$

The solution is:

$$\ln \frac{\phi}{1-\phi} + \ln e^{\xi\phi} = \eta \tag{D.11}$$

$$\ln \left(\frac{\phi}{1-\phi} e^{\xi\phi} \right) = \eta \tag{D.12}$$

$$\frac{\phi}{1-\phi}(1 + \xi\phi) = e^{\eta} \tag{D.13}$$

$$\xi\phi^2 + (1 + e^{\eta})\phi - e^{\eta} = 0 \tag{D.14}$$

$$\Delta = (1 + e^{\eta})^2 + 4\xi e^{\eta} \tag{D.15}$$

$$\phi_{1,2} = \frac{-(1 + e^{\eta}) \pm \sqrt{(1 + e^{\eta})^2 + 4\xi e^{\eta}}}{2\xi} \tag{D.16}$$

We expand the square root according to $\sqrt{1+x} = 1 + x/2 + x^2/8 + ...$ up to the third term and choose a positive sign in Eq. D.16. The negative sign gives a non-physical solution (concentration cannot be negative).

$$\begin{aligned} \phi = \frac{-(1 + e^{\eta})}{2\xi} + \frac{(1 + e^{\eta})}{2\xi} \left[1 + \frac{1}{2} \frac{4\xi e^{\eta}}{(1 + e^{\eta})^2} - \frac{1}{8} \frac{4^2 \eta^2 e^{2\eta}}{(1 + e^{\eta})^4} \right] = \\ = \frac{e^{\eta}}{1 + e^{\eta}} - \frac{\xi e^{2\eta}}{(1 + e^{\eta})^3} = \\ = \frac{e^{\eta}}{1 + e^{\eta} \left(1 - \frac{\xi e^{\eta}}{(1+e^{\eta})^2} \right)}. \end{aligned} \tag{D.17}$$

If we consider a case, when there is no interactions between components (inclusions), $\xi = 0$, we get

$$\ln \frac{\phi}{1-\phi} = \eta \tag{D.18}$$

$$\frac{\phi}{1-\phi} = e^{\eta} \tag{D.19}$$

$$\phi = \frac{e^{\eta}}{1+e^{\eta}} \tag{D.20}$$

Thus the Eq. (D.9) and has solutions (D.20) and (D.17) where

$$\eta = \frac{2K}{n_s kT}\left[(H_m^A - H_m^B)(H_m^B - H) + (D_m^A - D_m^B)(D_m^B - D) + \frac{\lambda}{2K}\right], \tag{D.21}$$

$$\xi = -\frac{2K}{n_s kT}\left[(H_m^A - H_m^B)^2 + (D_m^A - D_m^B)^2\right] \tag{D.22}$$

and in terms of curvatures

$$\eta = \frac{K}{n_s kT}\left[(C_{1m}^A - C_{1m}^B)(C_{1m}^B - C_1) + (C_{2m}^A - C_{2m}^B)(C_{2m}^B - C_2) + \frac{\lambda}{K}\right], \tag{D.23}$$

$$\xi = -\frac{K}{n_s kT}\left[(C_{1m}^A - C_{1m}^B)^2 + (C_{2m}^A - C_{2m}^B)^2\right] \tag{D.24}$$

Substituting η into Eq. (D.17) we get

$$\phi = \frac{e^{\frac{2K}{n_s kT}\left[(H_m^A - H_m^B)(H_m^B - H) + (D_m^A - D_m^B)(D_m^B - D) + \frac{\lambda}{2K}\right]}}{1 + e^{\frac{2K}{n_s kT}\left[(H_m^A - H_m^B)(H_m^B - H) + (D_m^A - D_m^B)(D_m^B - D) + \frac{\lambda}{2K}\right]}} \tag{D.25}$$

Eq. (D.25) is the general form for the function of concentration for two-component membrane.

References

[1] B. Alberts, A. Johnson, J. Lewis, M. Raff, K. Roberts, and P. Walter. *Molecular biology of the cell*. Garland Science, 2008.

[2] H. Gao, W. Shi, and L. B. Freund. Mechanics of receptor-mediated endocytosis. *PNAS*, 102:9469–9474, 2005.

[3] G. J. Doherty and H. T. McMahon. Mechanisms of endocytosis. *Annu. Rev. Biochem.*, 78:857 – 902, 2009.

[4] E. Gongadze, D. Kabaso, S. Bauer, T. Slivnik, P. Schmuki, U. van Rienen, and A. Iglič. Adhesion of osteoblasts to a nanorough titanium implant surface. *International journal of nanomedicine*, 6:1801–1816, 2011.

[5] D. Davis and S. Sowinski. Membrane nanotubes: dynamic long-distance connections between animal cells. *Molecular Cell Biology*, 9:431–436, 2008.

[6] K. Susuki. Myelin: a specialized membrane for cell communication. *Nature*, 3 (9):59, 2010.

[7] J. Israelachvili. *Intermolecular and Surface Forces*. Academic Press, London, 1991.

[8] R. Lipowsky and E. Sackmann. *Structure and Dynamisc of Membranes*. Elsevier, Amsterdam, 1995.

[9] C.R. Raetz, T.A. Garrett, C.M. Reynolds, W.A. Shaw, J.D. Moore, D.C. Smith, A.A. Ribeiro, R.C. Murphy, R.J. Ulevitch, C. Fearns, D. Reichart, C.K. Glass, C. Benner, S. Subramaniam, R. Harkewicz, R.C. Bowers-Gentry, M.W. Buczynski, J.A. Cooper, R.A. Deems, and E.A Dennis. Kdo2-lipid a of escherichia coli, a defined endotoxin that activates macrophages via tlr-4. *Lipid Res.*, 47:1097–111, 2006.

[10] H. Sasaki and S. H. White. Aggregation behavior of an ultra-pure lipopolysaccharide that stimulates tlr-4 receptors. *Biophys J.*, 95:986–93, 2008.

[11] H.S. Chung and C.R. Raetz. Interchangeable domains in the kdo transferases of escherichia coli and haemophilus influenzae. *Biochemistry*, 49:4126–37, 2010.

[12] M. S. Bretscher. Asymmetrical lipid bilayer structure for biological membranes. *Nature New Biology*, 236:11–12, 1972.

[13] S. J. Singer and G. L. Nicolson. The fluid mosaic model of the structure of cell membranes. *Science*, 175:720–731, 1972.

[14] M. B. Schneider, J. T. Jenkins, and W. W. Webb. Thermal fluctuations of large cylindrical phospholipid vesicles. *Biophys. J.*, 45:891 – 899, 1984.

[15] J. Hjort Ipsen, G. Karlström, O. G. Mouritsen, H. Wennerström, and M. J. Zuckermann. Phase equilibria in the phosphatidylcholine-cholesterol system. *Biochim. et Biophys. Acta*, 905:162 – 172, 1987.

[16] K. Bacia, P. Schwille, and T. Kurzchalia. Sterol structure determines the separation of phases and the curvature of the liquid-ordered phase in model membranes. *PNAS*, 102:3272 – 3277, 2005.

[17] K. Simons and E. Ikonen. Functional rafts in cell membranes. *Nature*, 387:569 – 572, 1997.

[18] A. Wieslander, A. Christiansson, L. Rilfors, and G. Lindblom. Lipid bilayer stability in membranes. regulation of lipid composition in acholeplasma laidlawii as governed by molecular shape. *Biochemistry*, 19:3650 – 3655, 1980.

[19] W. Rawicz, K. C. Olbrich, T. McIntosh, D. Needham, and E. Evans. Effect of chain length and saturation on elasticity of lipid bilayers. *Biophys. J.*, 79:328 – 339, 2000.

[20] P. Balgavý, M. Dubničkova, Norbert Kučerka, M. A. Kiselev, S. P. Yaradaikin, and D. Uhriková. Bilayer thickness and lipid interface area in unilamellar extruded 1,2-diacylphosphatidylcholine liposomes: a smell-angle neutron scattering study. *Biochimica et Biophisica Acta*, 1512:40 – 52, 2001.

[21] A. G. Lee. How lipids affect the activities of integral membrane proteins. *Biomembranes*, 1666:62 –87, 2004.

[22] A. Pralle, P. Keller, E. L. Florin, K. Simons, and J. K. Horber. *J. Cell. Biol.*, 148:997, 2000.

[23] G. J. Brewer. In vivo assembly of a biological membrane of defined size, shape, and lipid composition. *J. Virol.*, 30 (3):875 – 882, 1979.

[24] A. Moscho, O. Orwar, D. T. Chu, B. P. Modi, and R. N. Zare. Rapid preparation of giant unilamellar vesicles. *PNAS*, 93:11443 – 11447, 1996.

[25] E. Tani and N. Higashi. Myelin figures associated with tthe cytoplasmic membranes in human medulloblastoma. *Acta nueropath. (Berl.)*, 21:128–139, 1972.

[26] O. J. Castejón. Electrom microscopy of myelin figures in normal and pathological tissues. a review. *Acta Microscopica*, 17 (2):13 – 19, 2008.

[27] R. Lipowsky. Budding of membranes induced by intramembrane domains. *J. Phys. II France*, 2:1825–1840, 1992.

[28] U. Seifert. Curvature-induced lateral phase segregation in two-component vesicles. *Physical Review Letters*, 70:1335–1338, 1993.

[29] D. Andelman, T. Kawakatsu, and K. Kawasaki. Equilibrium shape of two-component unilamellar membranes and vesicles. *Europhysics Letters*, 19 (1):57–62, 1992.

[30] T. Kawakatsu, D. Andelman, K. Kawasaki, and T. Taniguchi. Phase transitions and shapes of two component membranes and vesicles i: strong segregation limit. *J. Phys. II France*, 3:971–997, 1993.

[31] F. Jülicher and R. Lipowsky. Shape transformations of vesicles with intramembrane domains. *Phys. Rev. E*, 53:2618, 1996.

[32] M. Fisher. *J. Phys. II (France)*, 3:1795–1805, 1993.

[33] J.B. Fournier. Nontopological saddle-splay and curvature instabilities from anisotropic membrane inclusions. *Phys. Rev. Lett.*, 76:4436–4439, 1996.

[34] V. Kralj-Iglič. *Eur. Biophys. J*, 24:311–321, 1996.

[35] A. Roux, D. Cuvelier, P. Nassoy, J. Prost, P. Bassereau, and B. Goud. Role of curvature and phase transition in lipid sorting and fission of membrane tubules. *EMBO Journal*, 24:1537 – 1545, 2005.

[36] T. Harder, C. Rentero, T. Zech, and K. Gaus. Plasma membrane segregation during t cell activation: probing the order of domains. *Curr Opin Immunol.*, 19:470–475, 2007.

[37] V. Kralj-Iglič, S. Svetina, and B. Zeks. The existence of non-axisymmetric bilayer vesicle shapes predicted by the bilayer couple model. *Eur. Biophys. J.*, 22:97–103, 1993.

[38] A. Iglič, P. Veranič, K. Jezernik, M. Fošnarič, B. Kamin, H. Hägerstrand, and V. Kralj-Iglič. Spherocyte shape transformation and release of tubular nanovesicles in human erythrocytes. *Bioelectrochemistry*, 62:159–161, 2004.

[39] Alina Ciach and Wojciech T. Góźdź. Nonelectrolyte solutions exhibiting structure on the nanoscale. *Annu. Rep. Prog. Chem., Sect. C*, 97:269 – 314, 2001.

[40] T. Baumgart, S. T. Hess, and W. W. Webb. Imaging coexisting fluid domains in biomembranes models coupling curvature and line tension. *Nature*, 425:821–824, 2003.

[41] W. T. Góźdź. Spontaneous curvature induced shape transformation of tubular polymersomes. *Langmuir*, 20:7385–7391, 2004.

[42] W. Helfrich. Elastic properties of lipid bilayers: Theory and possible experiments. *Z. Naturforsch*, 28c:693–703, 1973.

[43] A. Tian and T. Baumgart. Sorting of lipids and proteins in membrane curvature gradients. *Biophysical Journal*, 96:2676–2688, 2009.

[44] B. J. Peter, H. M. Kent, I. G. Milles, Y. Vallis, P. J. Butler, P. R. Evans, and H. T. McMahon. *Science*, 303:495, 2004.

[45] M. Heinrich, A. Tian, C. Esposito, and T. Baumgart. Dynamic sorting of lipids and proteins in membrane tubes with a moving phase boundary. *PNAS*, 107:7208–7213, 2010.

[46] Mahassine Safouane, Ludwig Berland, Andrew Callan-Jones, Benoit Sorre, Winfried Römer, Ludger Johannes, Gilman E. S. Toombes, and Patricia Bassereau. Lipid cosorting mediated by shiga toxin induced tubulation. *Traffic*, 11(12):1519–1529, 2010.

[47] Kerwyn Casey Huang and Kumaran S. Ramamurthi. Macromolecules that prefer their membranes curvy. *Molecular Microbiology*, 76(4):822–832, 2010.

[48] Johannes Ludger and Mayor Satyajit. Induced domain formation in endocytic invagination, lipid sorting, and scission. *Cell*, 142:507 – 510, 2010.

[49] Vikram Kjøller Bhatia, Nikos S. Hatzakis, and Dimitrios Stamou. A unifying mechanism accounts for sensing of membrane curvature by bar domains, amphipathic helices and membrane-anchored proteins. *Seminars in Cell and Developmental Biology*, 21(4):381 – 390, 2010.

[50] V. S. Markin. *Biophys. J.*, 36:1, 1981.

[51] S. Leibler. Curvature instability in membranes. *J. Phys. France*, 47:507–516, 1986.

[52] T. M. S. Chang. Semipermeable microcapsules. *Science*, 146:524 – 525, 1964.

[53] T. Baumgart, B. R. Capraro, C. Zhu, and S. L. Das. Thermodynamics and mechanics of membrane curvature generation and sensing by proteins and lipids. *Annu. Rev. Phys. Chem.*, 62:483–506, 2011.

[54] R.P. Rand and A.C. Burton. Mechanical properties of the red cell membrane: I. membrane stiffness and intracellular pressure. *Biophys. J.*, 4:115–135, 1964.

[55] Y.C. Fung. Theoretical considerations of elasticity of red cell and small blood vessels. *Federation Proceedings*, 25:1761, 1966.

[56] P.B. Canham. The minimum energy of bending as a possible explanation of the biconcave shape of the human red blood cell. *J. of Theor. Biol.*, 26:61–76, 1970.

[57] E. A. Evans. Bending resistance and chemically induced moments in membrane bilayers. *Biophys. J.*, 14:923–931, 1974.

[58] H. J. Deuling and W. Helfrich. Red blood cell shapes as explained on the basis of the curvature elasticity. *Biophys. J.*, 16:861 – 868, 1976.

[59] H. T. McMahon and J. L. Gallop. Membrane curvature and mechanisms of dynamic cell membrane remodelling. *Nature*, 438:590–596, 2005.

[60] J. Hurtig, D. T. Chiu, and B. Önfelt. Intercellular nanotubes: insights from imaging studies and beyond. *WIREs Nanomed Nanobiotechnol*, 2:260–276, 2010.

[61] A. Rustom, R. Saffrich, I. Markovic, P. Walther, and H.-H. Gerdes. Nanotubular highways for intercellular organelle transport. *Science*, 303:1007–1010, 2004.

[62] E. Lou, S. Fujisawa, A. Morozov, A. Barlas, Y. Romin, Y. Dogan, S. Gholami, A. L. Moreira, K. Manova-Todorova, and M. A. S. Moore. Tunneling nanotubes provide a unique conduit for intercellular transfer of cellular contents in human malignant pleural mesothelioma. *Plos One*, 7:e33093, 2012.

[63] W. Helfrich and J. Prost. Intrinsic bending force in anisotropic membranes made of chiral molecules. *Phys. Rev. A*, 38:3065 – 3068, 1988.

[64] T. M. Fischer. Bending stiffness of lipid bilayers. iii. gaussian curvature. *J. Phys. II France*, 2:337–343, 1992.

[65] E. A. Evans and R. Skalak. *Mechanics and thermodynamics of biomembranes*. J Biomech Eng, 1980.

[66] A. Iglič, B. Babnik, U. Gimsa, and V. Kralj-Iglič. On the role of membrane anisotropy in the beading transition of undulated tubular membrane structures. *J. Phys. A: Math. Gen.*, 38:8527–8536, 2005.

[67] V. Kralj-Iglič. Stability of membranous nanostructures: a possible key mechanism in cancer progression. *Interanational Journal of Nanomedicine*, 7:3579–3596, 2012.

[68] L. D. Landau and E. M. Lifshitz. *Theory of elasticity (Volume 7 of A Course of Theoretical Physics)*. Pergamon Press, 1970.

[69] W. T. Góźdź. Influence of spontaneous curvature and microtubules on the conformations of lipid vesicles. *J. Phys. Chem. B*, 109:21145–21149, 2005.

[70] J. J. Stoker. *Differential geometry*. Wiley-Interscience, Hoboken, New Jersey, U.S.A, 1969.

[71] W. T. Góźdź. The interface width of separated two-component lipid membranes. *J. Phys. Chem. B*, 110:21981–21986, 2006.

[72] U. Seifert, K Berndl, and R. Lipowsky. Shape transformations of vesicles: Phase diegram for spontaneous-curvature and bilayer-coupling models. *Phys. Rev. A*, 44:1182–1202, 1991.

[73] W. T. Góźdź, N. Bobrovska, and A. Ciach. Separation of components in lipid membranes induced by shape transformation. *The Journal of Chemical Physics*, 137:15101, 2012.

[74] Michael C. Heinrich, Benjamin R. Capraro, Aiwei Tian, Jose M. Isas, Ralf Langen, and Tobias Baumgart. Quantifying membrane curvature generation of drosophila amphiphysin n-bar domains. *The Journal of Physical Chemistry Letters*, 1(23):3401–3406, 2010.

[75] Benjamin R. Capraro, Youngdae Yoon, Wonhwa Cho, and Tobias Baumgart. Curvature sensing by the epsin n-terminal homology domain measured on cylindrical lipid membrane tethers. *Journal of the American Chemical Society*, 132(4):1200–1201, 2010.

[76] Deborah Kuchnir Fygenson, John F. Marko, and Albert Libchaber. Mechanics of micotubule-based membrane extension. 79:4497–4500, 1997.

[77] Wojciech T. Góźdź. Influence of spontaneous curvature and microtubules on the conformations of lipid vesicles. 109:21145–21149, 2005.

[78] Aurélien Roux, Gerbrand Koster, Martin Lenz, Benoît Sorre, Jean-Baptiste Manneville, Pierre Nassoy, and Patricia Bassereau. Membrane curvature controls dynamin polymerization. *PNAS*, 107(9):4141–4146, 2010.

[79] J. Käs and E. Sackmann. Shape transitions and shape stability of giant phospholipid vesicles in pure water induced by area-to-volume changes. *Biophys. J.*, 60(4):825–844, 1991.

[80] Udo Seifert. Curvature-induced lateral phase segregation in two-component vesicles. 70:1335–1338, 1993.

[81] F. Campelo and A. Hernández-Machado. Polymer-induced tubulation in lipid vesicles. *Phys. Rev. Lett.*, 100:158103, 2008.

[82] I. Derényi, F. Jülicher, and J. Prost. Formation and interaction of membrane tubes. *Physical Review Letters*, 88 (23):238101–1 – 238101–4, 2002.

[83] K. Farsad, N. Ringstad, K. Takei, S. R. Floyd, K. Rose, and P. De Camilli. Generation of high curvature membranes mediated dy direct endophilin bilayer interactions. *The Journal of Cell Biology*, 155 (2):193–200, 2001.

[84] Kazunari Akiyoshi, Ayako Itaya, Shin ichiro M.Nomura, Naoaki Ono, and Kenichi Yoshikawa. Induction of neuron-like tubes and liposome networks by cooperative e¡ect of gangliosides and phospholipids. *FEBS Letters*, 534:33 – 38, 2003.

[85] V. Kralj-Iglič, A. Iglič, H. Hägerstrand, and P. Peterlin. Stable tubular microvesicles of the erythrocyte membrane induced by dimeric amphiphiles. *Physical Review E*, 61:4230 – 4234, 2000.

[86] Aleš Iglič, Henry Hägerstrand, Peter Veranič, Ana Plemenitaš, and Veronika Kralj-Iglič. Curvature induced accumulation of anisotropic membrane components and raft formation in cylindrical membrane protrusions. *Journal of Theoretical Biology*, 240:368–373, 2006.

[87] N. Bobrovska, W.Góźdź, V. Kralj-Iglič, and A. Iglič. On the role of anisotropy of membrane components in formation and stabilization of tubular structures in multicomponent membranes. *PLoS ONE*, 8(9):e73941, 2013.

[88] D. Kabaso, N. Bobrovska, W. Góźdź, E. Gongadze, V.Kralj-Iglič, R. Zorec, and A. Iglič. The transport along membrane nanotubes driven by the spontaneous curvature of membrane components. *Bioelectrochemistry*, 87:204–210, 2012.

[89] D. Kabaso, N. Bobrovska, W. Góźdź, N. Gov, V. Kralj-Iglič, P. Veranič, and Al. Iglič. On the role of membrane anisotropy and bar proteins in the stability of tubular membrane structures. *J. Biomech.*, 45:231 – 238, 2012.

[90] T. G. D'Onofrio, A. Hatzor, A. E. Counterman, J. J. Heetderks, M. J. Sandel, and P. S. Weiss. Controlling and measuring the interdependence of local properties in biomembranes. *Langmuir*, 19:1618 – 1623, 2003.

[91] V. Kralj-Iglič, A. Iglič, M. Bobrowska-Hägerstrand, and H. Hägerstrand. Tethers connecting daughter vesicles and parent red blood cell may be formed due to ordering of anisotropic membrane constituents. *Colloids and Surfaces A*, 179:57 – 64, 2001.

[92] Y. Li, R. Lipowsky, and R. Dimova. Membrane nanotubes induced by aqueous phase separation and stabilized by spontaneous curvature. *PNAS*, 108:4731–4736, 2011.

[93] Gerbrand Koster, Martijn VanDuijn, Bas Hofs, and Marileen Dogterom. Mem tube formation from giant vesicles by dyanmic association of motor proteins. *PNAS*, 100:15583 – 15588, 2003.

[94] A. Roux, G. Cappello, J. Cartaud, J. Prost, B. Goud, and P. Bassereau. A minimal system allowing tubulation with molecular motors pulling on giant liposomes. *PNAS*, 99:5394 – 5399, 2002.

[95] P. Veranič, M. Lokar, G. J. Schütz, J. Weghbuger, S. Wieser, H. Hägerstrand, V. Kralj-Iglič, and A. Iglič. Different types of cell-to-cell connections mediated by nanotubular structures. *Biophysical Journal*, 95:4416–4425, 2008.

[96] A. Roux. The physics of membrane tubes: soft templates for studying cellular membranes. *Soft Matter*, 9:6726–6736, 2013.

[97] T. Allen and P.R. Cullis. Drug delivery systems: Entering the mainstream. *Science*, 303:1818 – 1822, 2004.

[98] M. Bally, K. Bailey, K. Sugihara, D. Grieshaber, J. Vörös, and B. Städler. Liposome and lipid bilayer arrays towards biosensing applications. *Small*, 6:2481–2497, 2010.

[99] W. Helfrich. Blocked lipid exchange in bilayers and its possible influence on the shape of vesicles. *Z. Naturforsch*, 29 c:510–515, 1974.